A rRNA hybridization-based approach for rapid and accurate identification of diverse fungal pathogens

Elizabeth A. Yee[1*] Brooks J. Burt[2*] Poppy C. S. Sephton- Clark[2,3] M. Lauren Donnelly-Morrell[1,4], Isaac H. Solomon[5], Evan Mojica[7], Christina A. Cuomo[1, 6#] Roby P. Bhattacharyya[1, 8#]

[1]Infectious Disease and Microbiome Program, Broad Institute of MIT and Harvard, Cambridge MA 02142 USA
[2]Genomic Center for Infectious Disease, Broad Institute of MIT and Harvard, Cambridge MA 02142 USA
[3]Valo Health, 75 Hayden Avenue Suite 200, Lexington, MA 02421 USA
[4]Department of Pathology, Massachusetts General Brigham, Harvard Medical School, Boston, MA USA
[5]Department of Pathology, Brigham and Women's Hospital, Harvard Medical School Boston, MA 02115 USA
[6]Department of Molecular Microbiology and Immunology, Brown University, Providence RI 02912 USA
[7]Microbiology Laboratory, Department of Pathology, Massachusetts General Hospital, Boston, MA 02114, USA
[8]Infectious Disease Division, Department of Medicine, Massachusetts General Hospital, Boston MA 02114 USA
*Denotes Co-First authorship EAY and BJB contributed equally.
[#]To whom correspondence should be addressed

Abstract

Invasive fungal infections are a global threat; early diagnosis is critical for patient outcomes, but current diagnostic measures remain notoriously slow. Here we extend our multiplexed, hybridization-based rRNA-targeted strategy for rapid, sensitive pathogen identification, previously designed for diverse bacteria and *Candida* species, to identify diverse fungal pathogens. We created a set of 91 probes targeting 86 medically relevant fungal species, designed to recognize regions of differential conservation across taxonomic groupings, from class- to species-specific probes. We assessed assay performance across a Training Set of 93 clinical isolates spanning 32 species of common fungal pathogens across 18 genera, with Pearson correlations of probeset reactivity profiles (PSRPs) accurately identifying the pathogen at the species, genus, and class level with 83%, 93%, and 94% accuracy, respectively, in a leave-one-out analysis. We developed a more sophisticated classifier on this Training Set, using taxonomic categories to select progressively more informative probes at each taxonomic level. After optimization, we assessed performance on an independent Validation Set of 54 clinical isolates spanning the same species as the Training Set, with 91%, 94%, and 98% at the species, genus, and family levels respectively. We piloted our assay on formalin-fixed paraffin-embedded (FFPE) tissue, demonstrating rapid, culture-independent fungal identification from this high-value clinical sample type, often the sole specimen available. The assay requires <30 minutes hands-on time (or <65 minutes from FFPE tissue), returning results in <8 hours from cultured specimen or FFPE tissue to answer on an RNA detection platform available in clinical laboratories.

Introduction

Invasive fungal infections (IFIs) are a growing threat to human health, accounting for 1.6 million global deaths annually.[1] Advances in immunosuppressive drugs and chemotherapy have resulted in larger immunocompromised populations vulnerable to opportunistic pathogens. [2–4] Early diagnosis of fungal infections is critical for patient outcome, but is notoriously slow, relying heavily on expert clinical mycologists identifying morphology from cultured or fixed patient specimens.[1,5,6] As such, healthcare systems are in need of rapid and accurate diagnostic tools to identify fungal infections.[3-5]

Progress has been made in fungal diagnostics using several different modalities. Serological testing can help diagnose IFIs by detecting fungal antigens, or host antibodies reflecting exposure, but many assays have cross reactivity.[7,8] Serology platforms often have a quick turnaround time and no culturing requirement, but are limited by a narrow species range or high false positivity rate for more general fungal markers such as 1,3-β-D-glucan.[3,7,9,10] Widely used for bacterial identification, matrix assisted laser desorption/ionization time of flight (MALDI-TOF) mass spectrometry is gaining traction as a method of fungal identification.[7,11,12,13] Although this method is easy to run, it requires culture growth which is not always possible, and identification is complicated by variable surface proteome expression across the fungal life cycle, making fungi harder to identify against reference databases.[5,7,14]

As costs fall and efficiency increases, sequencing is increasingly used for fungal identification. Targeted amplicon sequencing of the internal transcribed spacer region (ITS), ribosomal RNA genes (rDNA), or additional highly conserved genes has been widely adopted by reference laboratories to discriminate between fungal species.[5,9,15,16] However, fungal DNA in primary clinical samples is often very scarce, requiring amplification that can result in false positives from low-level contaminants.[17] Conversely, false negatives can occur due to inhibition of PCR

66 enzymes.[17] Despite these improvements in fungal diagnostics, no single strategy or commercial
67 test can identify a wide variety of fungal organisms rapidly and accurately. Additionally,
68 sequencing assays are often send-out tests with lengthy turnaround times, limiting their clinical
69 utility. There is thus a critical need to explore diagnostic options that balance sensitivity,
70 specificity, scalability, and breadth of coverage.
71
72 Previously, we described a novel rRNA-based strategy for rapid, sensitive bacterial identification
73 directly from primary clinical samples or cultured blood samples utilizing a commercially
74 available assay platform for multiplexed hybridization-based RNA quantification
75 (NanoString).[18,19] This assay, which we named phylogeny-informed rRNA-based strain
76 identification (Phirst-ID), uses 192 probes targeting regions in the 16S and 23S rRNA from 98
77 medically relevant bacterial species.[18] Each target region was selected for specificity at the level
78 of a pathogenic species, or higher taxonomic levels.[18] The fluorescent read-out from these
79 probes results in differential hybridization that creates a unique “fingerprint” pattern of reactivity
80 that accurately identifies each species.[18] We later extended this approach to yeast, designing a
81 Candida Phirst-ID probeset that discretely identified 11 medically relevant *Candida* species with
82 100% accuracy by targeting the 18 and 28S rRNA subunits.[20] By recognizing the highly
83 abundant rRNA itself, rather than the DNA that encodes it, this approach can detect and identify
84 <30 cells without amplification.[20]
85
86 Here we further expanded this approach by creating a panel of 91 probes targeting 86 medically
87 relevant fungi, targeting regions of the 18S and 28S rRNA subunits with differential conservation
88 across taxonomic groupings, ranging from class to species (**Fig. 1**). This species list targeted
89 the Fungal Priority Pathogen List from the WHO and intentionally excluded 56 common
90 environmental fungi as an outgroup in the design process. The resulting “Pan-Fungal Phirst ID”
91 assay was first tested on a curated Training Set of 93 clinical isolates, then verified on a

92 Validation Set of 54 independent isolates. Using Pearson correlations, we achieved a positive
93 species match rate of 84%. For some isolates, higher order taxonomic probes dominated the
94 signature, compromising accuracy by overpowering more specific signals from genus and
95 species level probes. To address this, we developed an optimized classifier, increasing species-
96 level accuracy to 89%. To assess potential utility on primary specimens, we piloted the assay on
97 archived clinical formalin-fixed paraffin-embedded (FFPE) tissue samples.
98
99 **Materials and Methods:**
100 **Probeset Design**
101 We compiled a comprehensive list of medically relevant fungi, using the WHO Fungal Priority
102 Pathogen list as a guide, for training and validation of our probeset. We collated the 18S and
103 partial 28S sequences for 86 medically relevant fungal species primarily from the Silva
104 database; where sequences were too short or not available, we retrieved regions from NCBI
105 assemblies for the following: *Mucor circinelloides*, *Emergomyces orientalis*, *Epidermophyton*
106 *floccosum*, *Coccidioides posadasii*, *Coccidioides immitis*, *Histoplasma capsulatum*,
107 *Emergomyces pasteurianus*, *Exophiala dermatitidis*, *Trichophyton indotiniae*, *Kodamaea*
108 *ohmeri*, *Wickerhamomyces anomalus*, *Kluyveromyces marxianus*, *Malassezia dermatis*,
109 *Enterocytozoon bieneusi*. Additional 18S sequences were selected from Silva for 56
110 environmental fungal species to serve as an outgroup during probe design to minimize
111 unintentional cross reactivity. Due to inconsistent annotation of the 28S sequences, we were
112 unable to obtain full-length 28S sequences for all ingroup species. For outgroup species, we
113 were only able to obtain reliable 18S sequences. We compiled a full taxonomic classification of
114 each species (**Fig. S1, Table S1**). Employing a similar strategy used in the Pan-Bacterial Phirst-
115 ID probeset design[18]. We profiled each desired target sequence using NanoString's proprietary
116 probe design algorithm to identify all putative pairs of consecutive 50mer probe-binding regions
117 that meet parameter specifications. Specifically, probe sequences are assessed for predicted

118 binding kinetics, thermodynamics, secondary structure, and sequence composition for the
119 desired targets while minimizing predicted cross-reactivity against non-targeted outgroup
120 species, or the human genome. For species-specific probes, outgroups included and all other
121 pathogenic and environmental fungi; we sought probes predicted to bind exclusively to the
122 targeted species in a given rRNA region, whose sequence was unique to that species (**Table**
123 **S2**). For probes targeting higher taxa (genus, family, order, or class), we sought probes
124 predicted to bind all members of that taxon, (including either pathogen or environmental fungi,
125 since including only pathogens would likely impose unrealistic constraints in sequence space),
126 while excluding all outgroups not belonging to that taxon. For *Candida* species, which have
127 undergone considerable phylogenetic reclassification of late, we kept the clinically familiar
128 genus classification *Candida* for all (*Candida, Candidozyma, Pichia, Nakeseomyces,*
129 *Meyerozyma*, etc.), which likely changed design constraints on the genus-level probe. This
130 decision could be revisited in future iterations of the probeset.
131
132 The final probeset includes 60 probes designed to be species-specific, as well as 31 probes
133 designed to recognize rRNA regions conserved across higher taxonomic groupings, including
134 14 genus-level probes, 8 family probes, 5 order probes, and 4 class probes (**Fig. S1**). During
135 testing, the *Mucor circinelloides* 28S probe yielded substantial cross-reactivity against nearly all
136 tested species. We thus removed this probe analytically, resulting in a final set of 91 probes
137 used for all analyses (**Table S1**). Also included in the probeset are 12 control probe pairs (6
138 negative, 6 positive) directed at External RNA Controls Consortium (ERCC) targets as
139 previously described.[18] The 6 positive controls are directed at ERCC spike-ins included in every
140 hybridization reaction at pre-specified concentrations; the 6 negative controls are directed at
141 biorthogonal targets not included in the hybridization.
142
143

144 **Sample acquisition**

145 Most of our clinical isolates were collected from the Massachusetts General Hospital (MGH)
146 Clinical Microbiology Laboratory, for both Training and Validation Sets. These isolates were
147 provided as cell pellets suspended in Trizol solution after culture isolation on standard fungal
148 media in the clinical laboratory. Isolates were identified through standard clinical microbiology
149 workflows as part of routine patient care and shared with the investigators under Mass General
150 Brigham Institutional Review Board protocol 2015P002215. In keeping with diagnostic
151 limitations in these standard clinical workflows, some isolates were only identified to the genus
152 level, including all *Curvularia*, *Coccidioides*, *Fusarium*, *Cunninghamella*, *Mucor*, *Rhizopus* and
153 *Talaromyces* isolates. Some *Candida* species were supplemented from our own laboratory
154 collection and the Antibiotic Resistance Isolate Bank drug resistant *Candida* (CAN) and *Candida*
155 *auris* (CAU) collections. Additional samples were generously shared with us from the following
156 sources: *Histoplasma capsulatum* cell pellets suspended in Trizol from Dr. Sinem Beyhan
157 (JCVI)[21], *Pneumocystis jirovecii* gDNA from human autopsy samples from Dr. Joseph Kovacs
158 (NIH), and *Blastomyces dermatiditis* purified RNA*, Cryptococcus gattii, Paracoccidioides*
159 *brasiliensis, Sporothrix schenckii* and *Talaromyces marneffei* purified gDNA from the Fungal
160 Genomics Group at the Broad Institute.[21–25] Per our biosafety regulations, all cultured isolates
161 from external collaborators were received in Trizol. If we were unable to obtain a cultured
162 isolate, we utilized either gDNA or RNA as available. Coded/de-identified FFPE tissue samples
163 were obtained from the Brigham & Women's Hospital (BWH) Pathology Department, after visual
164 screening to identify archived clinical samples from 2019-2025 with varying levels of visible
165 fungal forms (ranging from rare to confluent). Fungal identification of these autopsy and surgical
166 pathology cases were based on integration of all available laboratory results from anatomic
167 pathology histochemical stains, culture isolation from concurrently collected tissue samples, and
168 molecular testing of FFPE tissue, frozen tissue, or culture isolates.[26] **Table S3** lists all samples
169 and sources.

170

171 **Training and Validation Set parameters**

172 To test the Pan-Fungal Phirst-ID probeset, we acquired as many samples from our fungal
173 pathogen list as possible. In all, we collected 171 samples (isolates, gDNA, or RNA) from 53
174 species. To assess assay performance as rigorously as possible, we divided these samples into
175 Training and Validation Sets based on the number of samples of each species we were able to
176 collect (**Table S3a, b**). In the ideal case, we included 3 samples of the same genus and species
177 in the Training Set, with any remaining samples (up to 3 more) used for validation. If we were
178 only able to obtain 3 samples total, we included 2 in the Training Set and kept the third in the
179 Validation Set (**Table S3a, b**). In the end, this led to 93 samples across 33 species in the
180 training set, with 54 samples across 32 species in the Validation Set. For 21 additional species,
181 we were only able to obtain 1 (n = 18) or 2 (n = 3) samples. Since this was insufficient to
182 assess classification accuracy, we did not include these samples in either the Training or
183 Validation Sets, but we do report their results separately. For assessment of classification
184 performance, background subtraction and normalization was carried out exactly as previously
185 described,[18,20] and classifiers were developed and iterated using only data from the Training
186 Set, before being run on the Validation Set with no changes to any analytical processes. All
187 Validation Set analyses were done with authors blinded to sample identification until after
188 predictions were finalized. For FFPE samples, pathology co-authors (MLD-M and IHS) selected
189 samples, whereas the remaining co-authors (notably EAY, BJB, CAC, RPB) stayed blinded to
190 the identities of all species until all thresholding decisions, classification algorithms, and identity
191 predictions were finalized.

192 **Sample processing**

193 <u>Cultured isolates collected from MGH</u>

194 Clinical isolates were received from the clinical microbiology laboratory in Trizol and processed
195 as follows: 125µL of each sample in Trizol was added to a 2ml screw cap tube (MP

196 Biomedicals, CAT# 76044-692) with an additional 125µL of Trizol reagent (ThermoFisher
197 CAT#15596026) with 100µl of 0.1uM zirconia/silica beads (Biospec, CAT# 11079101z), then
198 bead-beaten for 2 rounds on the FastPrep 5G (MP Biosciences) for 90s, at 10 m/s. 50µL of
199 chloroform was added to each sample, inverted, and the mixture was spun down at 12,000 x g
200 for 15 minutes at 4C. 50µL of the aqueous phase was transferred to a fresh 1.5 ml Eppendorf
201 tube. To prevent degradation of the RNA in this crude lysate, 50µL RLT buffer (Qiagen CAT#
202 79216) with 1% β-mercaptoethanol (β-ME), an irreversible chemical RNase inhibitor, was added
203 to each lysate prior to storage at -80ºC.

204 gDNA samples of selected isolates

205 gDNA samples from the Fungal Genomics group at the Broad Institute were used to assist in
206 species coverage for members of the Fungal Priority Pathogen list. Approximate concentrations
207 were measured using the Nanodrop One system (ThermoFisher CAT#ND-ONE-W). Dilutions of
208 some gDNA samples were made in 1x Phosphate Buffered Saline (PBS) to ensure probe
209 reactivity patterns were within control cutoffs and max probe limits as described below.

210 Cultured isolates prepared from ARBank isolates

211 The ARBank *C. auris* (CAU) and drug-resistant *Candida* (CAN) collections were used to
212 supplement *Candida* species for Training and Validation sets (**Table S3a, b**). Cultured isolates
213 prepared in house and were processed as previously described.[20]

214

215 **NanoString Data generation**

216 Our custom Pan-Fungal Phirst-ID probeset was run using the Elements assay variation on the
217 standard NanoString assay for multiplexed RNA detection. Briefly, lysates from cultured
218 organisms were diluted first at a 1:10 ratio in PBS to avoid assay saturation. For gDNA and
219 RNA samples, dilution was not always necessary depending on the concentration of the
220 sample. For all samples, 1.5µL of lysate or nucleic acid was incubated with unlabeled probe
221 pairs for each target (IDT) and Elements TagSet-96 reagents (NanoString CAT#121000608).

222 Hybridization conditions were standard, except for 2 modifications: lysates were incubated at 95
223 °C for 2 minutes immediately prior to hybridization to denature secondary structural elements
224 and disrupt protein binding in rRNA targets, and hybridizations were incubated for one hour
225 instead of the recommended 16-24 hours, exactly as we have previously done[18,20]. Hybridized
226 samples were then run on the NanoString nCounter platform and subsequently analyzed using
227 the nCounter Digital Analyzer.
228
229 Cell densities from samples cultured by collaborators, and from paraffin scrolls, were unknown
230 prior to running on the nCounter platform. We established three parameters to address sample
231 overloading: (1) positive control signals out of the expected order given known spike-in
232 concentrations, suggesting cross-reactivity; (2) any negative control value > 100 total read
233 counts; or (3) maximum probe count >100,000, where saturation might affect relative ratios. If
234 any of these 3 parameters were met, the affected sample was re-run with increased dilutions
235 until the issue resolved. The maximum number of re-runs required for a given sample was up to
236 three to meet our stated parameters. Across training and Validation Sets, 62 lysates required at
237 least one re-run, with four samples requiring additional runs. All such decisions were made
238 solely based on these three criteria, prior to any assessment of prediction accuracy.
239
240 **Data processing and visualization**
241 Raw binding data (counts per probe) were compiled using NanoString nSolver software (v3.0).
242 Raw counts were normalized using positive and negative control spike-ins provided by
243 NanoString using custom scripts in R, and background signal for each probe was subtracted
244 based on the average of three blank lanes, exactly as previously described.[18] Pearson
245 correlations for the resulting normalized, background-subtracted probeset reactivity profiles
246 were subsequently calculated across samples using the “cor” function in R (version 4.3.1).

247 Heatmaps were generated by the Pheatmap package v1.0.12 in R. Probes and samples were
248 arranged phylogenetically.
249
250 **Co-PILOT Classification**
251 We developed a hierarchical classification model based on Pearson correlations (**Fig. S4**)
252 termed **Co**mplementarity-based **P**hylogeny-**I**nformed **L**evel-**O**riented **T**raversal (Co-PILOT),
253 coded entirely in R (version 4.3.1 github) Initial Pearson correlations were calculated for each
254 isolate to identify most similar samples based on probe-binding signatures. The taxonomic
255 group (starting with class) was then found for the closest match. All other isolates not in this
256 taxonomic group were then removed, as were probes not specific to that group (**Fig. S4a-b**).
257 This process was repeated until the species level, or if there were no more samples to compare
258 to. The Co-PILOT algorithm was developed and iterated using only our Training Set, then
259 deployed without modification on our Validation Set, considering each Validation sample one at
260 a time and using matches to the Training Set as its basis for identification decisions. When the
261 best match was to a sample from the MGH clinical laboratory for which identification was only
262 determined to the genus level, Co-PILOT was unable to make a species prediction but could
263 predict identity to the genus level.
264
265 **Pilot study of FFPE samples**
266 FFPE scrolls (60µm per block in each tube) were obtained from the Brigham and Women's
267 Hospital Pathology Department. Samples FP001-FP012, FP016-019 were processed using the
268 RNeasy FFPE kit (Qiagen CAT# 73504), per NanoString recommendations. Given inconsistent
269 results at an interim assessment, we processed the remaining samples (FP020-030) using the
270 quick DNA/RNA FFPE kit (Zymo CAT# R1009) (**Table S3c**). Samples were first deparaffinized
271 using proprietary deparaffinization solutions provided by each kit followed by heating tissue to
272 either 56ºC followed by 80ºC (Qiagen) or 54ºC (Zymo), separating wax from tissue. Prior to

273 moving to column purification, samples underwent two rounds of bead beating as described
274 previously and spun down at 13,000xg for 1 min before loading onto column for final purification.
275 All lysates were stored at -80ºC after elution. FFPE samples were analyzed as a separate
276 dataset relative to Training and Validation Sets. Compiled FFPE data was analyzed for species
277 classification against a "superset" containing Training, Validation, and rare incidence isolate
278 datasets, mirroring how we would expect to deploy this method on primary tissue samples going
279 forward. After visual inspection of resulting PSRPs for all samples, we had low confidence in
280 samples that had <1000 raw counts from any probe (see **Fig. S9**). Using this metric as a
281 baseline, we divided samples based on their max probe counts into low and high confidence
282 groups, though we report Co-PILOT's best match for each sample in each group. As described
283 above, if a species identification was not defined for a given sample, the final best match was
284 made at the genus level.
285
286 **ITS sequencing workflow to confirm species ID**
287 Clinical isolates were received in Trizol, and additional cultured material was unavailable. For
288 those unable to be identified to the species level by standard workflows, we sought to obtain
289 genomic DNA (gDNA) to enable ITS sequencing. As these samples were intended for extraction
290 of RNA rather than DNA, we omitted the chloroform extraction, which improves partitioning of
291 RNA from gDNA, hoping this would result in enough gDNA for PCR. 100µL of remaining
292 inactivated sample not used in original lysate prep was combined with an additional 300µL of
293 Trizol, then underwent 2 rounds of bead beating as previously described, then processed using
294 the Zymo DirectZol RNA kit (CAT#: R2050). Samples were eluted in 25ul of Elution buffer as
295 specified. ITS1 and ITS2 regions were amplified using the NEB Q5 hot start master mix
296 (CAT#:M0491S) using primers and cycling conditions as previously described.[20,27] PCR
297 products were visualized on an E-Gel Power Snap Electrophoresis Device (Invitrogen
298 CAT#:G8100) using a 1% Agarose E-Gel (Invitrogen CAT#: G401001) for the presence of

299 bands for ITS1 or ITS2. Samples with bands corresponding to either ITS1, ITS2 or both were
300 purified using the Zymo DNA Clean and Concentrate (CAT#: D4033) and sent to Plasmidsaurus
301 for amplicon sequencing. Results were first analyzed in Geneious and trimmed for quality using
302 standard parameters; trimmed sequences then were submitted to UNITE using the regular
303 output style and 2 sequence alignments per sample for analysis.[28]
304
305 **Results**
306 **Pathogen selection and Pan-Fungal Phirst-ID probeset design**
307 We selected 86 medically relevant fungi using the WHO Priority Pathogen List as key species to
308 target with our panel, and an outgroup of 56 environmental and non-medically relevant fungi
309 (**Table S1**). Targeting species-specific variable regions of the 18 and 28S rRNA subunits, we
310 designed 61 species-specific probes, one of which was removed from analyses due to
311 excessive cross-reactivity (see Methods). For the remaining targeted species, we could not
312 design a species-specific probe within the constraints of the NanoString assay due to
313 phylogenetic constraints. For the closely related *Candida albicans* and *Candida dubliniensis,*
314 and *Aspergillus fumigatus* and *Aspergillus clavatus,* we designed single probes predicted to
315 selectively recognize each pair of species.
316
317 As previously described,[18] we also designed higher-order taxonomic probes to improve
318 accuracy in identifying target species through multiple recognition events, creating a unique
319 probeset reactivity profile (PSRP) that serves as a “fingerprint” for each isolate tested. These
320 higher taxonomic order probes can also enable partial characterization of pathogens not
321 included in probeset design.[18] To do so, we analyzed the 18 and 28S sequences for variable
322 regions shared across species of the same genus, family, order, or class conserved enough to
323 recognize all members within a given taxonomic classification, while excluding outgroup

324 species.[18,20] This resulted in 14 genus probes, 8 family probes, 5 order probes and 4 class
325 probes, culminating in a Pan-Fungal Phirst-ID probeset of 91 probes (**Fig. 1**; **Fig. S1, Table S2**).
326
327 **Collation of Training and Validation Sets**
328 To rigorously test our panel, we collected isolates from 18 of 19 members of the WHO Fungal
329 Priority Pathogen List, as well as 35 other clinically important species available from the MGH
330 clinical microbiology laboratory. Isolates were split into Training and Validation Sets based on
331 availability, with three isolates per species used for Training when possible and all remaining
332 isolates used for Validation; when only three total isolates were available, two were used for
333 Training and one for Validation (**Table S3a, b**; see Methods). Our Training Set contains 93
334 isolates spanning 18 unique genera and 26 defined species, and our Validation Set contains 54
335 isolates with the same genus and species numbers. For 7 genera, we were unable to get
336 species characterization from the MGH clinical lab, due to standard clinical identification
337 methodology. In addition, we collected several clinical isolates that were too rare (n = 1 or 2 in
338 our collection) to include in our Training and Validation rubric. Though unable to rigorously
339 validate classification performance, we tested 24 of these isolates, spanning an additional 14
340 genera and 21 species not included in our Training and Validation Sets (**Fig. S2**).
341
342 **Unique reactivity profiles accurately distinguish species**
343 To quantify differences in PSRPs between species, we first calculated a pairwise Pearson
344 correlation coefficient for each sample against every other sample in the Training Set (**Fig. S3**).
345 This simple analytical approach incorporates data from all probes tested in the probeset across
346 the entire reactivity profile. Because of sequence conservation patterns in rRNA genes, PSRPs
347 of this probeset should reflect species identity. The strongest correlations should exist within
348 isolates of the same species, whereas non-species matched pairs should have lower correlation
349 coefficient (**Fig. 2**).[18,20] In a “leave one out” analysis for all isolates in the training set, 83%

350 matched best to members of the same species, with most mismatches occurring to closely
351 related species (**Fig. 3**). For 15 samples not identified to the species level, the best match in all
352 15 was to the same genus, the closest available taxonomic match in the Training Set. In all,
353 93% of isolates matched at the genus level, and match rates steadily increased for broader
354 taxa, reaching 100% at the class level (**Fig. 3a**).
355
356 **Leveraging taxonomy level information to improve classification accuracy**
357 For many isolates in our training set, the higher taxonomic order probes resulted in greater
358 signal than the species-specific probes (**Fig. 4a**). One notable example is the *Aspergillus* genus,
359 where class probes dominated the signal readout compared with species probes (**Fig. 4b**). This
360 systematic difference in probe binding by taxonomic level of the probe target, despite perfect
361 complementarity between probe and target, was not observed in bacteria.[18] This posed a
362 unique challenge to accurate classification by Pearson correlation, which intrinsically weights
363 higher signals and thus undervalues species-level probes with lower maximal reactivities,
364 reducing species-level accuracy.
365
366 To address this uneven signal distribution across probes targeting different taxonomic levels, we
367 developed a hierarchical classifier, still based on Pearson correlations but progressing stepwise
368 through taxonomic classifications. We called this classifier **Co**mplementarity-based **P**hylogeny-
369 **I**nformed **L**evel-**O**riented **T**raversal (Co-PILOT). This approach begins with the full PSRP, but
370 traverses down the taxonomic classification, at each step eliminating any species and probes
371 not included in the best-matched taxon. **Fig S4** illustrates a specific example of how Co-PILOT
372 analyzes an *Aspergillus* sample, narrowing from all probes and samples (**Fig. S4a**), through
373 class (best match = *Eurotiomycetes*), order (*Eurotiales*), and family (*Aspergillaceae*)-specific
374 ones (**Fig. S4b-d**), to only those from the *Aspergillus* genus (**Fig. S4e**). At each level, only
375 probes and samples relevant to the selected taxon are used to recalculate Pearson correlation

376 coefficients. The best-matched sample from the Training Set at the final step, usually at the
377 species level, is taken as Co-PILOT's final identification. If the best match from the Training Set
378 is a clinical sample only identified to the genus level (e.g., *Mucor* spp.), then Co-PILOT's final
379 step would be at the genus level. In this manner, the entire probeset is still used to classify each
380 sample, but at each taxonomic level, only the probes designed to be informative in
381 distinguishing among members of that taxon are considered. This method allows these more
382 precise reactivity patterns to inform identity, rather than idiosyncratic differences between
383 higher-order probes that might otherwise dominate a Pearson correlation. Critically, this novel
384 classifier was devised and iteratively refined based only on the Training Set, before data from
385 the Validation Set was examined. Thus, although Co-PILOT improved classification accuracy for
386 the Training Set (**Fig. S5**), this should be viewed as "over-trained". However, its performance on
387 the Validation Set represents an independent assessment of classification accuracy.
388
389 **The Pan-Fungal Phirst ID assay accurately classifies an independent Validation Set of**
390 **diverse fungal pathogens**
391 Fifty-four independent clinical isolates, representing the same genera and species as the
392 Training Set, were tested as a Validation Set for the Pan-Fungal Phirst-ID assay (**Fig. S6**). The
393 resulting PSRPs for these isolates were compiled into a separate dataset that was only released
394 for analysis after the entire Training Set had been analyzed and the Co-PILOT algorithm had
395 been finalized. Pearson correlations identified a similar fraction of species (85%) and higher-
396 order taxa in the Validation Set as the Training Set (**Fig. 5a, b**). Co-PILOT performed better,
397 identifying 89.3% of species in this independent Validation Set, with 96.2% concordance at the
398 family level and >98% for all higher-order taxa (**Fig. 5c**).
399 **Investigation of discrepant classifications in the Validation Set**
400 In the Validation Set, Co-PILOT misidentified 4 samples out of 54, all among species also
401 misidentified in leave-one-out analysis in the Training Set. Incorrect ID matches were correctly

402 binned at high order taxonomic levels but mismatched to different but related genera or species.
403 Specifically, misclassifications were made between *Cryptococcus neoformans* and
404 *Cryptococcus gattii*, and between *Scedosporium apiospermum* and *Lomentospora prolificans*.
405 Both pairs are closely related phylogenetically; *C. gattii* was formerly referred to as a serovar of
406 *C. neoformans,*[29,30] and *L. prolificans* was formerly classified as a *Scedosporium*.[31] In examining
407 reactivity profiles (**Fig. 2, Fig. S6**), despite probes designed to distinguish between each
408 species pair, no real distinction exists between their PSRPs. For the pair of *Cryptococcus*
409 species, a probe designed to selectively recognize the *C. gattii* 28S rRNA subunit failed to
410 generate a signal for either species. This *C. gattii* species-specific probe matches a *C.*
411 *deuterogattii* (VGII) sequence. Our training set included one *C. deuterogattii* sample, but this did
412 not react with the species-specific probe, suggesting this probe has a general binding issue and
413 should be redesigned and confirmed for alignment and potential reactivity to the other *C. gattii*
414 species complex members. For *S. apiospermum* and *L. prolificans*, two problems arose in these
415 closely related species: a probe designed to be specific for the *L. prolificans* 28S subunit cross-
416 reacted with *S. apiospermum* as strongly as with *L. prolificans*; whereas a probe designed to
417 selectively recognize the *S. apiospermum* 18S subunit generated no signal for either species.
418 Relevant family and class probes recognized both species comparably, as expected.
419
420 We investigated one additional discrepant classification in the Validation Set, which both
421 Pearson correlations and Co-Pilot called a *Rhizopus*, but the clinical identification labeled it a
422 *Mucor*. On visual inspection, its reactivity pattern clearly resembled the *Rhizopus* from our
423 Training Set more than the *Mucor* (**Fig. S7**). Given the difficulty in clinically distinguishing
424 among the *Mucorales* by morphology,[32,33] we pursued ITS sequencing to clarify, which showed
425 100% match to *Rhizopus microsporus* (**Table S3b**), not a *Mucor* species, consistent with our
426 assay's call. Reclassifying this isolate as a *Rhizopus* instead of a *Mucor* improves the accuracy

427 of our Co-Pilot classifications on the Validation Set (to 91%, 94%, and 98% at the species,
428 genus, and family levels respectively).
429
430 **Pilot use of Pan-Fungal Phirst-ID on clinical Formalin- Fixed Paraffin- Embedded (FFPE)**
431 **tissue samples**
432 Fixation of tissues using formalin and embedding in paraffin blocks is the gold standard method
433 for preparing human tissues for histopathologic diagnosis, including microorganism
434 identification.[34,35,36] However, this process prevents subsequent growth of microbes; thus, if
435 infection is only suspected after tissue fixation (e.g., in a lung nodule removed for suspicion of
436 neoplasia), culture-based pathogen identification is precluded. Often such samples are obtained
437 via surgical procedures that are impractical or even dangerous to repeat, meaning pathogen
438 identification must be done either imprecisely by morphology, or via nucleic acid extraction and
439 PCR from the fixed tissue.[37,38] Since Pan-Fungal Phirst-ID requires only hybridization and no
440 enzymology, we hypothesized that it might perform comparably to PCR on crude nucleic acid
441 preparations from FFPE tissue. We thus investigated the performance of our Pan-Fungal Phirst-
442 ID probeset on nucleic acids extracted from archived clinical FFPE samples on which fungal
443 forms were observed via microscopic examination, plus two negative controls with no fungal
444 forms (**Fig. S8**). Pan-Fungal Phirst-ID correctly identified FFPE samples, largely depending on
445 the quality of sample and NanoString read counts we were able to extract from each sample.
446 When plotting heatmaps of read counts, 55% displayed visually poor probe binding behavior;
447 thus, prior to running Co-PILOT, we opted to exclude these as non-informative and focus our
448 analysis on samples with sufficient NanoString reads (**Fig. S9**)**.** Of the 12 “high confidence”
449 samples, 8 were correctly identified, with 2 others notably close: an *A. fumigatus* was called *A.*
450 *clavatus*; and a *Madurella tropicana*, not included in our expanded Training Set, matched with
451 the closest possible phylogenetic match, an environmental *Chaetomium* isolate). We also found
452 a negative control with a large *Candida albicans* signature (**Fig. 6**), a possible contaminant in

453 sample collection or processing; the other negative control showed low signal as expected (**Fig.**
454 **S9**).
455
456 **Discussion**
457 Fungal infections are a growing global health problem, and current diagnostic methods are
458 unable to meet the demands of healthcare systems. Currently available testing measures have
459 significant limitations from financial burdens for instrument costs or expert personnel, frequent
460 false positives for biomarkers, and limited organism range for which specific tests are available.
461 We previously developed a molecular diagnostic approach based on rRNA hybridization, Phirst-
462 ID, to rapidly and accurately identify bacterial pathogens[18] and *Candida* species[20] using a
463 commercial detection system present in clinical pathology laboratories primarily for oncological
464 use.[39–41] Here, we extended this approach to target 86 medically relevant fungi in our Pan-
465 Fungal Phirst-ID panel.
466
467 rRNA is an appealing target for hybridization-based identification due to its extreme
468 conservation within species,[42] and its high abundance, allowing amplification-free detection.
469 Experimental conditions for Phirst-ID only require base pairing, enabling detection from crude
470 lysate with <30 minutes hands-on time and no nucleic acid extraction or purification, with a total
471 assay time of <8 hours.[18] By comparison, we previously reported a median of 28 hours from
472 culture to identification for *Candida* bloodstream infections;[20] other fungi take longer to identify.
473 Unlike amplification-based methods, the lack of enzymology makes Phirst-ID compatible with
474 chemical RNase inhibitors for robust RNA stabilization. And whereas mass spectrometry-based
475 methods must contend with surface proteomes that can vary across the fungal life cycle [5,7,9,14]
476 rRNA is invariant.
477

478 Prior iterations of Phirst-ID identified organisms based on the closest Pearson correlation of
479 PSRPs of a query organism to that of organisms in a reference panel.[18,20] By contrast, upon
480 extending this approach to diverse fungal pathogens, we found that systematic variations in
481 probe intensity across the Pan-Fungal Phirst-ID panel led to avoidable errors using this
482 relatively simplistic classification scheme (**Fig. 4**). We therefore designed Co-PILOT, a classifier
483 that integrates Pearson correlations of full and partial PSRPs with known taxonomic
484 relationships between species to improve classification accuracy (**Fig. S4**). After iteratively
485 designing Co-PILOT based on a Training Set of 93 isolates across 32 species of common
486 fungal pathogens, Co-PILOT improved identification on an independent Validation Set of 54
487 isolates representing the same species compared with the simpler scheme. Two pairwise
488 misidentifications were made at the species level, each between close phylogenetic relatives:
489 Co-PILOT mistook *C. neoformans* for *C. gattii* and vice-versa, and *S. apiospermum* for *L.*
490 *prolificans* and vice-versa. Both errors appeared to be due to probes designed to distinguish
491 each pair, not performing as expected. In the former case, the distinction between *C.*
492 *neoformans* and *C. gattii* has minimal clinical consequences; though their geographic
493 distribution is somewhat distinct, and their propensity to infect immunocompetent patients may
494 somewhat differ, they both cause similar types of illness, with similar severity and management
495 options.[43] By contrast, the latter case is more clinically critical: though they cause a similar
496 spectrum of illness in similarly immunocompromised patients, the intrinsic antifungal resistance
497 profiles of *S. apiospermum* and *L. prolificans* differ meaningfully, leading to different empiric
498 therapies.[44,45] In order to distinguish these, iterations on the probeset would be required, and if
499 no rRNA-directed probe is able to make this clinically important distinction, mRNA targets may
500 be needed, at a cost of assay sensitivity; or a separate diagnostic test may be required.
501
502 In a pilot study to test additional clinical sample types on our Pan-Fungal Phirst-ID probeset, we
503 tested archived FFPE tissue samples containing fungal forms. This sample type is critical for

504 patient diagnosis when cultures are either not attempted or negative, or to identify species prior
505 to culture, which for fungi can take days to weeks.[1,5,6,37,38] FFPE tissue is optimized for
506 morphological examination, but molecular methods are increasingly used to identify
507 pathogens.[38] Typical workflows involve DNA extraction followed by rDNA-directed PCR with
508 amplicon sequencing, which generally has limited success, ranging from 13-34% in published
509 series,[46–50] typically worse for fungi.[47] Of the 27 FFPE samples we tested, 12 passed our
510 threshold of confidence (>1000 raw max probe counts); of these, Co-PILOT correctly identified
511 5 to the species level, 9 to the genus level, and one more to the closest available phylogenetic
512 match (**Fig. 6**). For 14 samples positive for fungal forms by microscopy, we were unable to
513 identify an organism due to lack of signal. Adding a bead beating step after deparaffinization
514 helped increase signal for some samples, but more work is required to optimize RNA extraction
515 for best results on this clinically important sample type, before testing head-to-head against the
516 current standard of practice.
517
518 This study has several limitations. First, although Pan-Fungal Phirst-ID was designed to detect
519 86 fungal pathogens, we have thus far only been able to rigorously test and independently
520 validate it against multiple isolates of 32 species. Its accuracy in identifying these 32 key
521 species should be well-predicted by its performance on our Validation Set and should improve
522 as the Training Set gets larger with further use. However, its performance on species not
523 included in this Training Set is uncertain. First, we did observe predictable recognition patterns
524 on an additional 18 species (**Fig. S2**), for which we were only able to obtain 1-2 examples for
525 testing. When trained on sufficient examples of new species, Pan-Fungal Phirst-ID should
526 perform well, as long as the 91 probes provide a unique PSRP. However, recognizing when an
527 off-panel species is encountered remains a key challenge. Second, although Pan-Fungal Phirst-
528 ID with Co-PILOT accurately identified >90% of clinical isolates samples to the species level
529 and 98% at the family level in an independent Validation Set, it clearly struggled with the

530 clinically relevant distinction between *S. apiospermum* and *L. prolificans*. Third, several isolates
531 in our Training and Validation Set were only identified to the genus level by the clinical
532 microbiology laboratory, and therefore Phirst-ID accuracy could only be measured to the genus
533 level. With further training, it is possible that species-level distinctions could be made, but
534 genus-level identification for these isolates meets or even exceeds current clinical laboratory
535 reporting standards for these genera (e.g., *Mucor*, *Rhizopus*, and *Cunninghamella* are often
536 reported as order *Mucorales* from clinical laboratories), whereas Pan-Fungal Phirst-ID
537 accurately identified them to the genus level - better than clinical morphology-based
538 assessments in at least one case (**Fig. S7**). Fourth, aside from the pilot on FFPE tissue, we thus
539 far only trained and tested this assay on monocultures. Although *Candida* Phirst-ID was able to
540 recognize mixed cultures as linear combinations of PSRPs from each species,[20] the increased
541 complexity of PSRPs in the Pan-Fungal probeset will likely make this more challenging. Fifth, in
542 this initial work, we rigorously tested this assay primarily on cultured isolates, although the
543 hybridization-based assay in other contexts has worked well despite an excess of off-target
544 nucleic acids (such as human tissue). Still, despite some promising results on a small number of
545 pilot samples, further optimization is needed for deployment on primary clinical samples,
546 including the high-value clinical use case of FFPE tissue. Finally, this assay is currently
547 research-use-only, like its bacterial and *Candida* counterparts. However, this broad-range,
548 sensitive assay could be readily applied to agricultural, environmental or biodefense monitoring.
549 It would be feasible to combine our bacterial probeset[18] with this Pan-Fungal probeset to
550 characterize complex samples or polymicrobial infection.[20] Additional work beyond the scope of
551 our academic laboratory would be required to optimize process and reagents, and ideally
552 automate portions of the workflow, prior to broader scope implementation. Once optimized and
553 scaled, Pan-Fungal Phirst-ID offers a novel approach to fungal identification that combines the
554 lack of enzymology of mass spectrometry with the invariant and high-abundance targets of
555 rRNA-based methods, implementable on either cultured isolates or primary specimens.

Acknowledgments:

We thank Dr. Sinem Beyhan and Jacob Durazo from the J. Craig Venter Institute, Dr. Joseph Kovacs, Dr. Shelly Curran, and Dr. Liang Ma from the NIH for generously sharing samples with us, and Andrew Grootsky, Aleksandr Kutchma, Richard Boykin (current or former employees of NanoString, now Bruker Spatial Biology, the company that manufactures the RNA detection platform used in this manuscript) for their assistance with our non-standard probe design. This work was supported in part by the National Institute of Allergy and Infectious Diseases and the National Institutes of Health [grant numbers 1R01AI153405 to R.P.B. and C.A.C., and T32 AI007061 to E.A.Y]. The content is solely the responsibility of the authors and does not necessarily represent the official views of the National Institutes of Health. The funders had no role in study design, data collection, and interpretation, or decision to submit this work for publication. R.P.B, E.A.Y and M.L.D-M are co-inventors on subject matter in BI-11335, and R.P.B is a co-inventor on subject matter in BI-11339, filed by the Broad Institute directed to methodology of identifying fungal pathogens using rRNA and disclosure of fungal probes, respectively, as described in this manuscript.

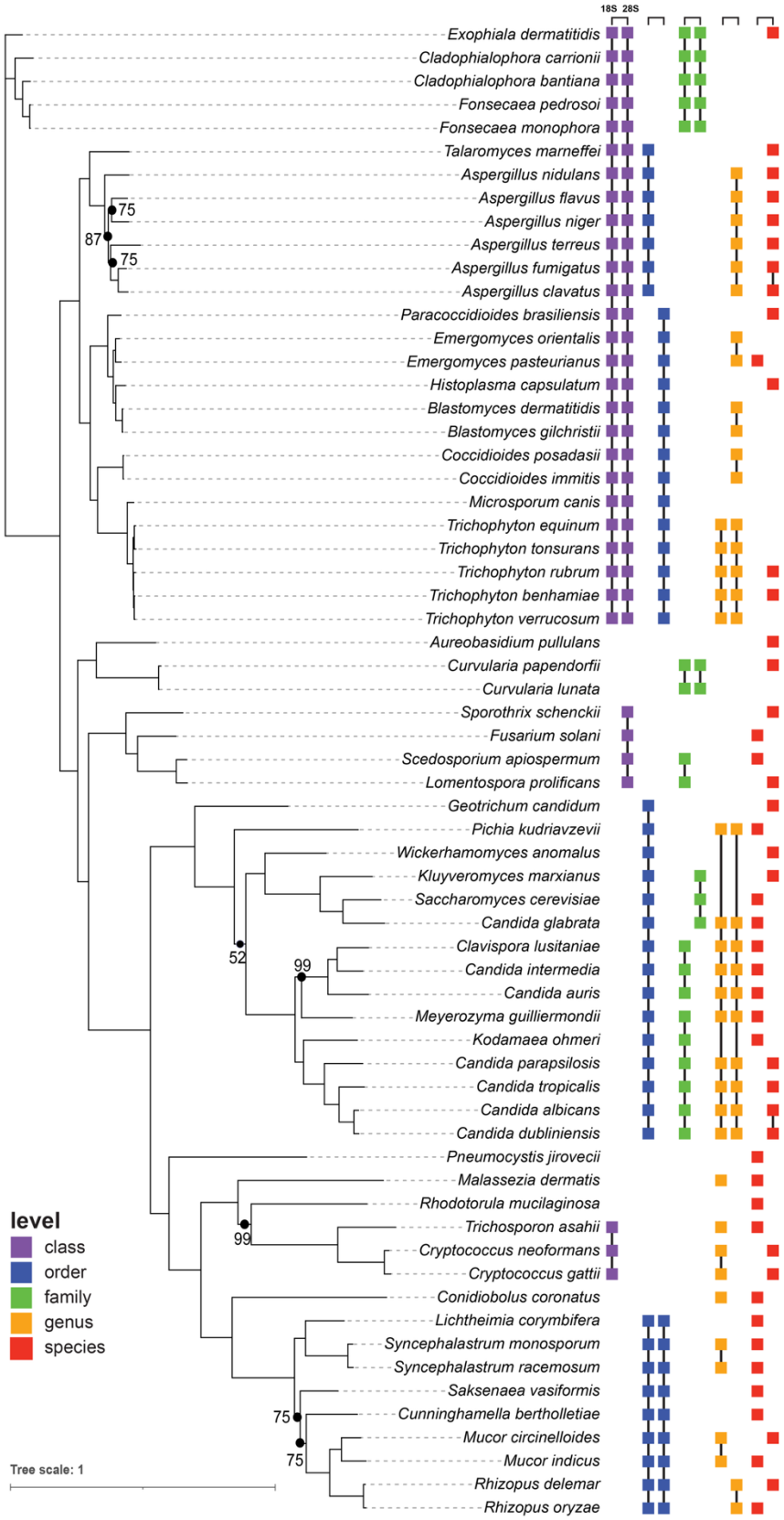
18S
28S
Exophiala dermatitidis
Cladophialophora carrionii
Cladophialophora bantiana
Fonsecaea pedrosoi
Fonsecaea monophora
Talaromyces marneffei
Aspergillus nidulans
Aspergillus flavus
Aspergillus niger
Aspergillus terreus
Aspergillus fumigatus
Aspergillus clavatus
Paracoccidioides brasiliensis
Emergomyces orientalis
Emergomyces pasteurianus
Histoplasma capsulatum
Blastomyces dermatitidis
Blastomyces gilchristii
Coccidioides posadasii
Coccidioides immitis
Microsporum canis
Trichophyton equinum
Trichophyton tonsurans
Trichophyton rubrum
Trichophyton benhamiae
Trichophyton verrucosum
Aureobasidium pullulans
Curvularia papendorfii
Curvularia lunata
Sporothrix schenckii
Fusarium solani
Scedosporium apiospermum
Lomentospora prolificans
Geotrichum candidum
Pichia kudriavzevii
Wickerhamomyces anomalus
Kluyveromyces marxianus
Saccharomyces cerevisiae
Candida glabrata
Clavispora lusitaniae
Candida intermedia
Candida auris
Meyerozyma guilliermondii
Kodamaea ohmeri
Candida parapsilosis
Candida tropicalis
Candida albicans
Candida dubliniensis
Pneumocystis jirovecii
Malassezia dermatis
Rhodotorula mucilaginosa
Trichosporon asahii
Cryptococcus neoformans
Cryptococcus gattii
Conidiobolus coronatus
Lichtheimia corymbifera
Syncephalastrum monosporum
Syncephalastrum racemosum
Saksenaea vasiformis
Cunninghamella bertholletiae
Mucor circinelloides
Mucor indicus
Rhizopus delemar
Rhizopus oryzae
75
87
75
52
99
99
75
75
level
class
order
family
genus
species
Tree scale: 1

576

Figure 1. Phylogenetic coverage of Pan-Fungal Phirst-ID probeset. Fungal species included in probeset design, arranged by maximum-likelihood phylogeny inferred using IQ-TREE. To the right of each species, each solo square or set of connected squares denotes a unique probe; black lines connecting squares indicate a single probe designed to target multiple species within a taxonomic group. Colors indicate taxonomic level of the probes (see key at bottom left). For each level, squares at left indicate an 18S rRNA target and at right a 28S rRNA target. Tree branch lengths are in expected substitutions per site.

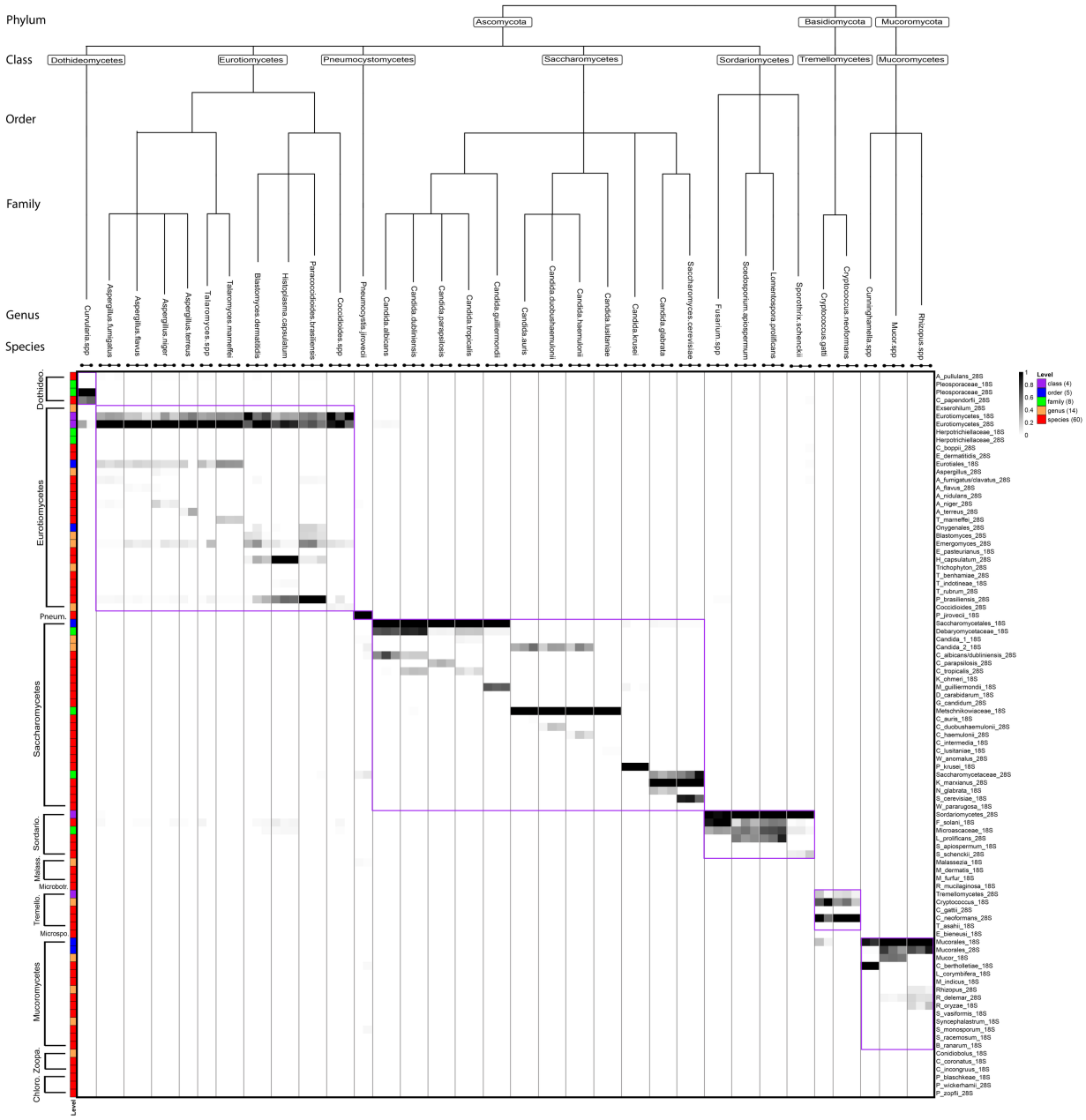

Figure 2. Pan-Fungal Phirst-ID panel generates unique PSRPs for 33 clinically relevant species. Heatmap shows scaled binding intensities of 91 probes (vertical axis) tested against the Training Set of 94 samples from 33 species (horizontal axis). Taxonomic level of each probe is indicated by colored box at left (numbers in parentheses = total probes designed at each level); probe name is listed at right. Each axis is ordered by taxonomic hierarchy, with species displayed in a cladogram. Horizontal black bars with dots indicate unique isolates of each species tested; vertical lines indicate transitions between species. Purple boxes indicate regions where the class of samples and intended probe targets match.

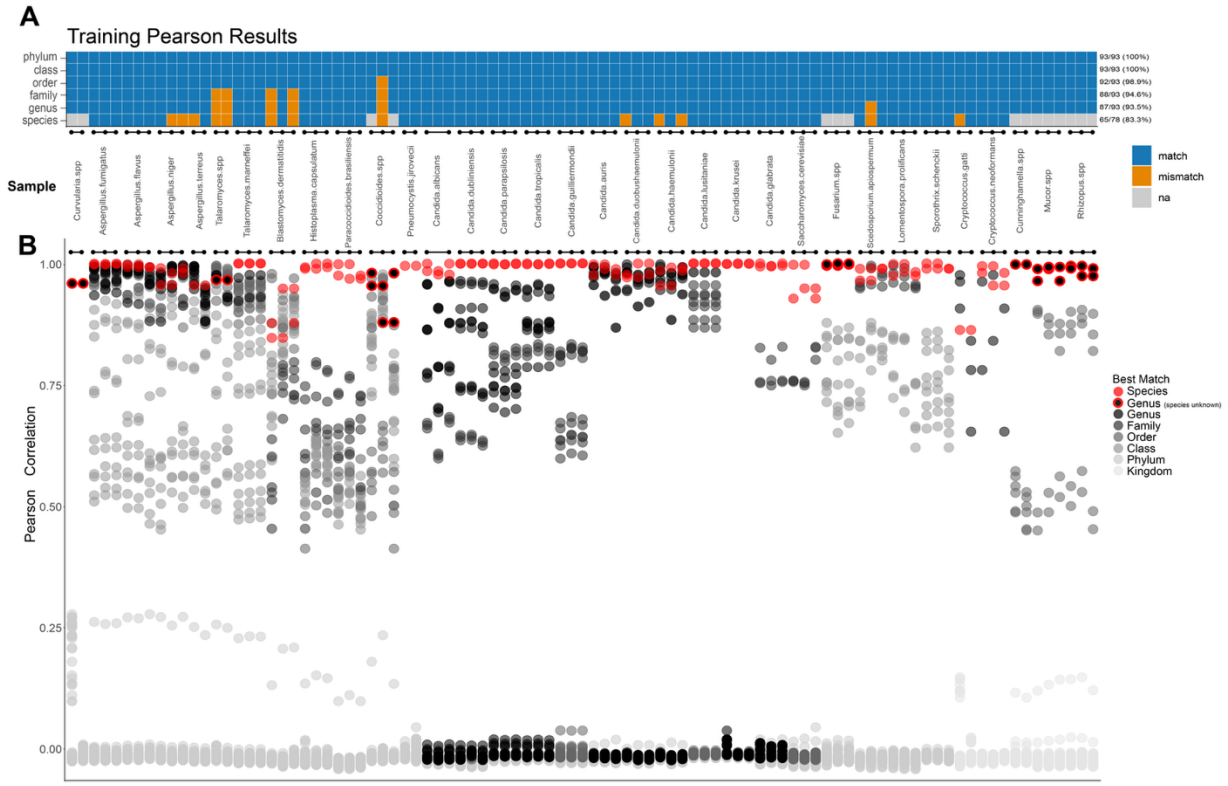

Figure 3. Pan-Fungal Phirst-ID PSRPs identify most species. Leave-one-out analysis of Training Set data showing closest taxonomic matches based on highest Pearson correlation. **(A)** Tile plot indicating accuracy of best non-self matches within the Training Set for identifying each individual isolate at each taxonomic level. **(B)** Dot plot of Pearson correlations of each indicated sample against all other samples in the Training Set, colored by closest-matched taxonomic level of the comparator. When the species of a test strain was unknown, the best possible match is to the genus level, indicated by a gray box at the species level in (A), and by a black circle with red border in (B).

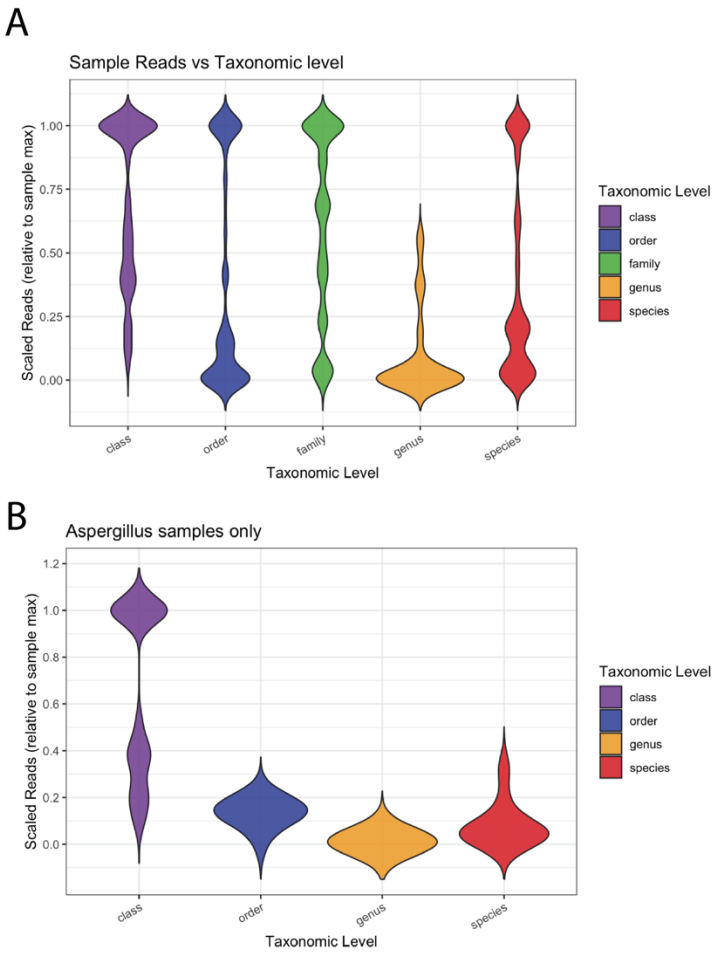

Figure 4. Probes designed for regions conserved at higher taxonomic levels exhibit higher binding signal. Violin plots of normalized signal intensity of probes targeting each taxonomic level of **(A)** all samples in Training Set and **(B)** only *Aspergillus* samples in Training Set. Y-axis for both graphs indicates non-zero probe reactivities normalized to the maximally reactive probe for each sample.

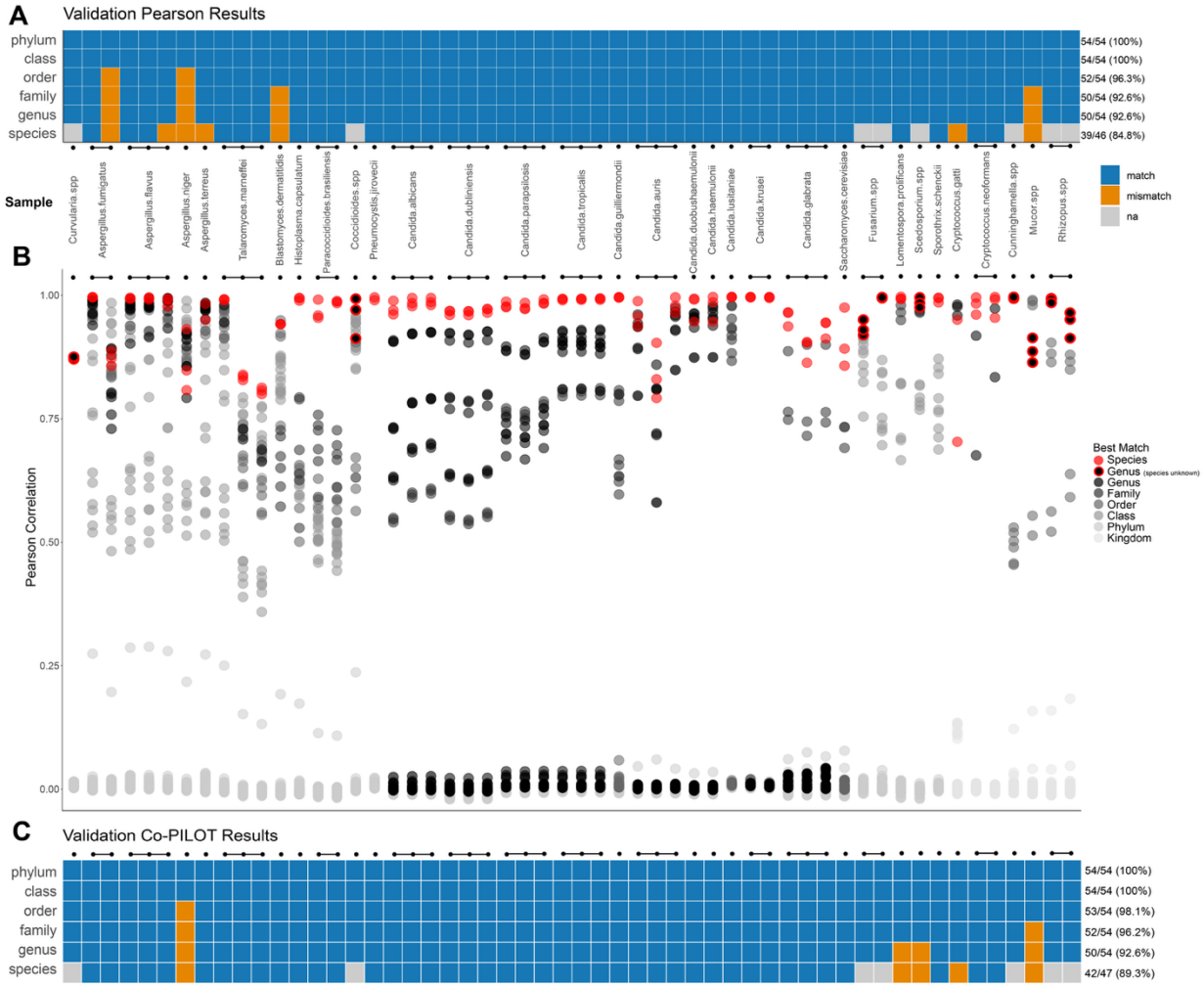

Figure 5: Pan-Fungal Phirst-ID PSRPs identify most species in independent Validation Set. Each sample in the Validation Set was compared by Pearson correlation with that of the entire Training Set. **(A)** Tile plot indicating accuracy of best matches at each taxonomic level based on highest Pearson correlation. **(B)** Dot plot of Pearson correlations of each Validation sample against all samples in the Training Set, colored by closest taxonomic level of the comparator. **(C)** Tile plot shows that Co-PILOT improves accuracy relative to simple Pearson correlations (A) for identifying the best match. When the species of a test strain was unknown, the best possible match is to the genus level, indicated by a gray tile at the species level in (A and C), and by a black circle with red border in (B).

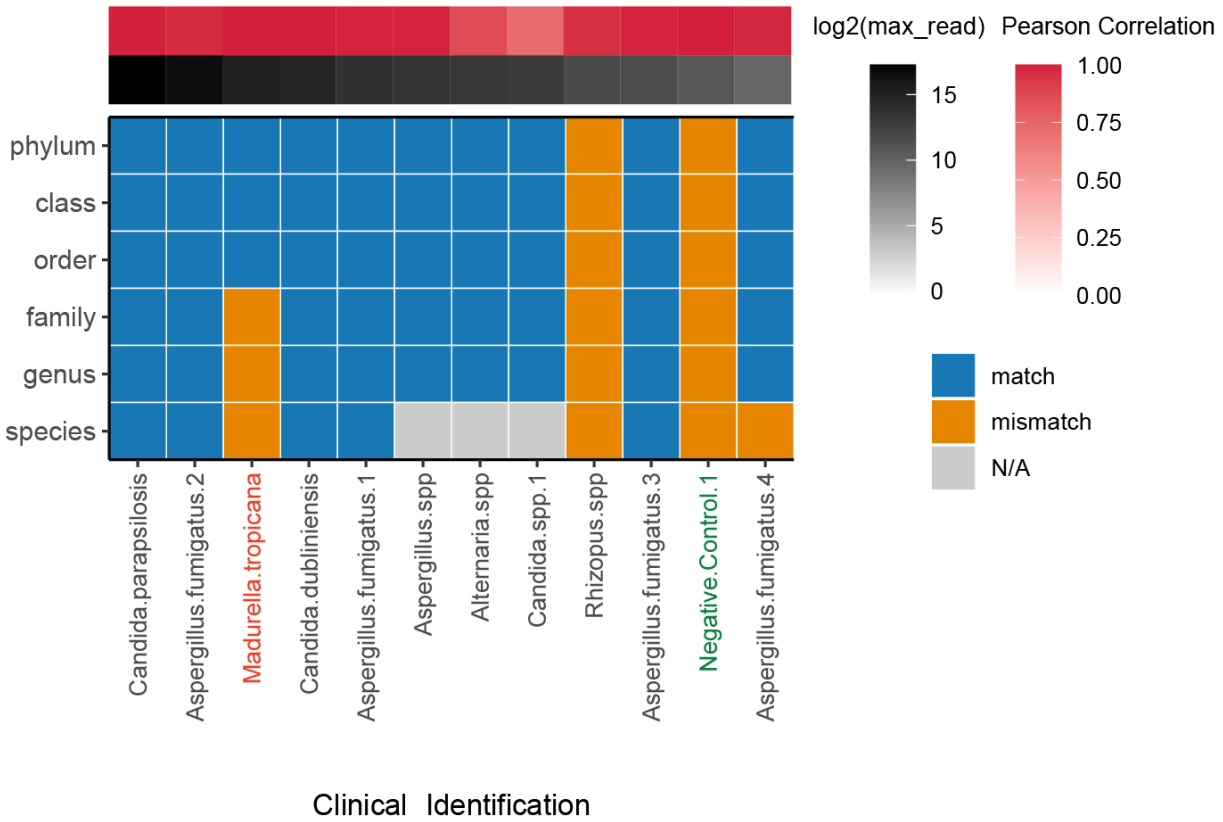

Figure 6. Pilot application of Pan-Fungal Phirst-ID to FFPE samples. Tile plot indicating prediction accuracy at each taxonomic level for the subset of FFPE samples with high enough probe reactivity to pass our threshold for Co-PILOT analysis. Sample order is based the highest probe read count (green heatmap), which was used to set this threshold. Red heatmap shows Pearson correlation of each sample to its best match. Clinical laboratory identifications are listed below (see Table S3c); red text indicates an organism not previously tested by Pan-Fungal Phirst-ID (and thus not available to Co-PILOT algorithm for comparison), green text = negative control FFPE sample (no fungal forms seen).

Figure S1. Coverage maps of Pan-Fungal Phirst-ID probe sequences along 18S and 28S rRNA subunits. Probe sequences mapped along target rRNA sequence of (A) 18S and (B) 28S subunits. Color of line indicates taxonomic level specificity of probe. Longer mappings indicate gaps in alignment due to

genetic variation in the consensus sequence. Light gray vertical lines indicate 500 bp distance along the consensus 18/28S axes (including gaps). Probe sequences are available in Supplementary Table S2.

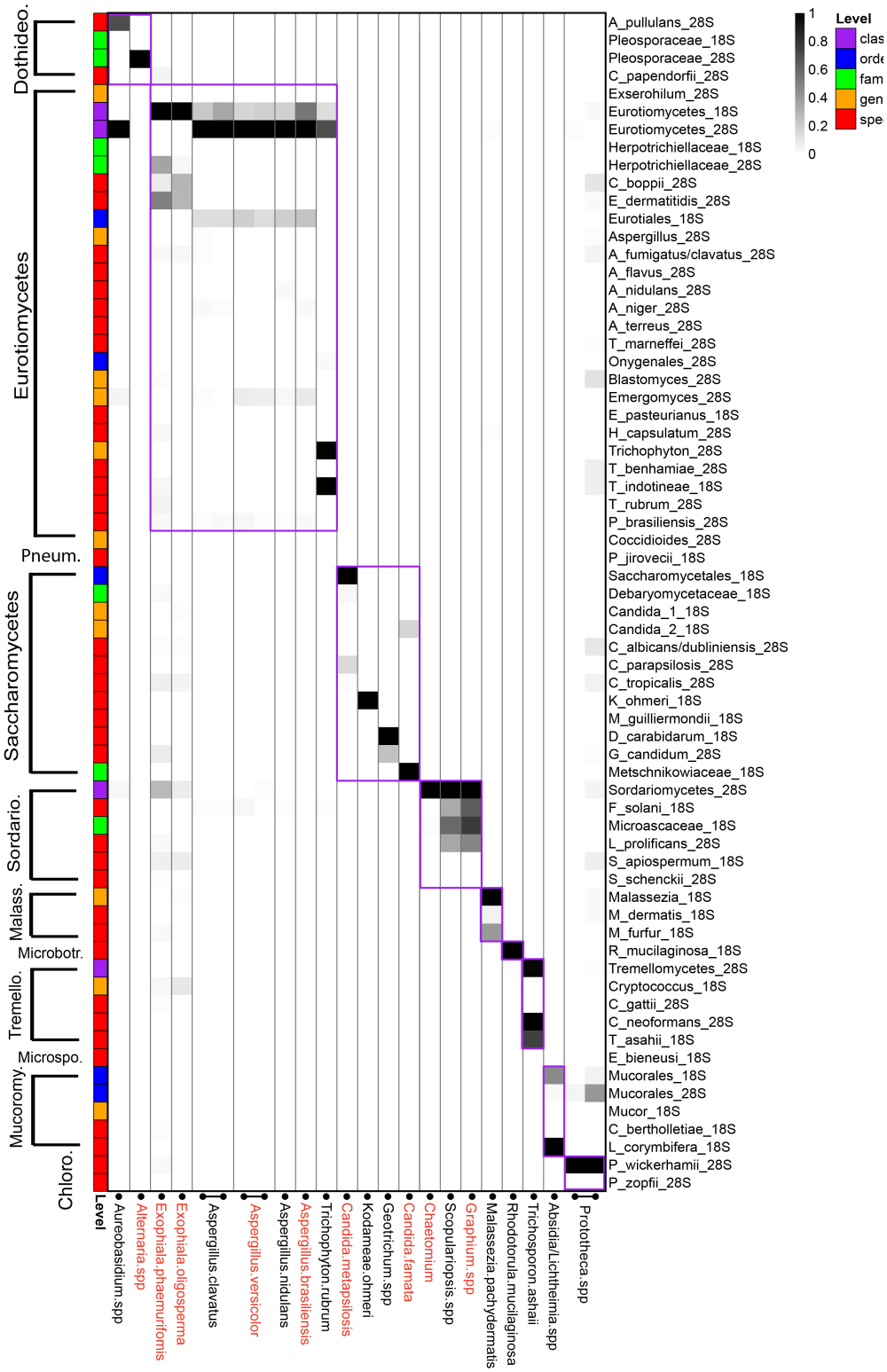
Level
clas
orde
fam
gen
spe
1
0.8
0.6
0.4
0.2
0
A_pullulans_28S
Pleosporaceae_18S
Pleosporaceae_28S
C_papendorfii_28S
Exserohilum_28S
Eurotiomycetes_18S
Eurotiomycetes_28S
Herpotrichiellaceae_18S
Herpotrichiellaceae_28S
C_boppii_28S
E_dermatitidis_28S
Eurotiales_18S
Aspergillus_28S
A_fumigatus/clavatus_28S
A_flavus_28S
A_nidulans_28S
A_niger_28S
A_terreus_28S
T_marneffei_28S
Onygenales_28S
Blastomyces_28S
Emergomyces_28S
E_pasteurianus_18S
H_capsulatum_28S
Trichophyton_28S
T_benhamiae_28S
T_indotineae_18S
T_rubrum_28S
P_brasiliensis_28S
Coccidioides_28S
P_jirovecii_18S
Saccharomycetales_18S
Debaryomycetaceae_18S
Candida_1_18S
Candida_2_18S
C_albicans/dubliniensis_28S
C_parapsilosis_28S
C_tropicalis_28S
K_ohmeri_18S
M_guilliermondii_18S
D_carabidarum_18S
G_candidum_28S
Metschnikowiaceae_18S
Sordariomycetes_28S
F_solani_18S
Microascaceae_18S
L_prolificans_28S
S_apiospermum_18S
S_schenckii_28S
Malassezia_18S
M_dermatis_18S
M_furfur_18S
R_mucilaginosa_18S
Tremellomycetes_28S
Cryptococcus_18S
C_gattii_28S
C_neoformans_28S
T_asahii_18S
E_bieneusi_18S
Mucorales_18S
Mucorales_28S
Mucor_18S
C_bertholletiae_18S
L_corymbifera_18S
P_wickerhamii_28S
P_zopfii_28S
Dothideo.
Eurotiomycetes
Pneum.
Saccharomycetes
Sordario.
Malass.
Microbotr.
Tremello.
Microspo.
Mucoromy.
Chloro.
Level
Aureobasidium.spp
Alternaria.spp
Exophiala.phaeomuriformis
Exophiala.oligosperma
Aspergillus.clavatus
Aspergillus.versicolor
Aspergillus.nidulans
Aspergillus.brasiliensis
Trichophyton.rubrum
Candida.metapsilosis
Kodameae.ohmeri
Geotrichum.spp
Candida.famata
Chaetomium
Scopulariopsis.spp
Graphium.spp
Malassezia.pachydermatis
Rhodotorula.mucilaginosa
Trichosporon.ashaii
Absidia/Lichtheimia.spp
Prototheca.spp

Figure S2 Pan-Fungal Phirst-ID PSRPs against additional samples not included in the Training Set. Heatmap displaying normalized probe binding intensities of 24 additional samples, for which we were only able to obtain 1 or 2 examples and thus did not meet criteria for inclusion in the Training or Validation Sets (because we could not rigorously apply our sample identification algorithms). Purple boxes indicate regions where the class of samples and intended probe targets match.

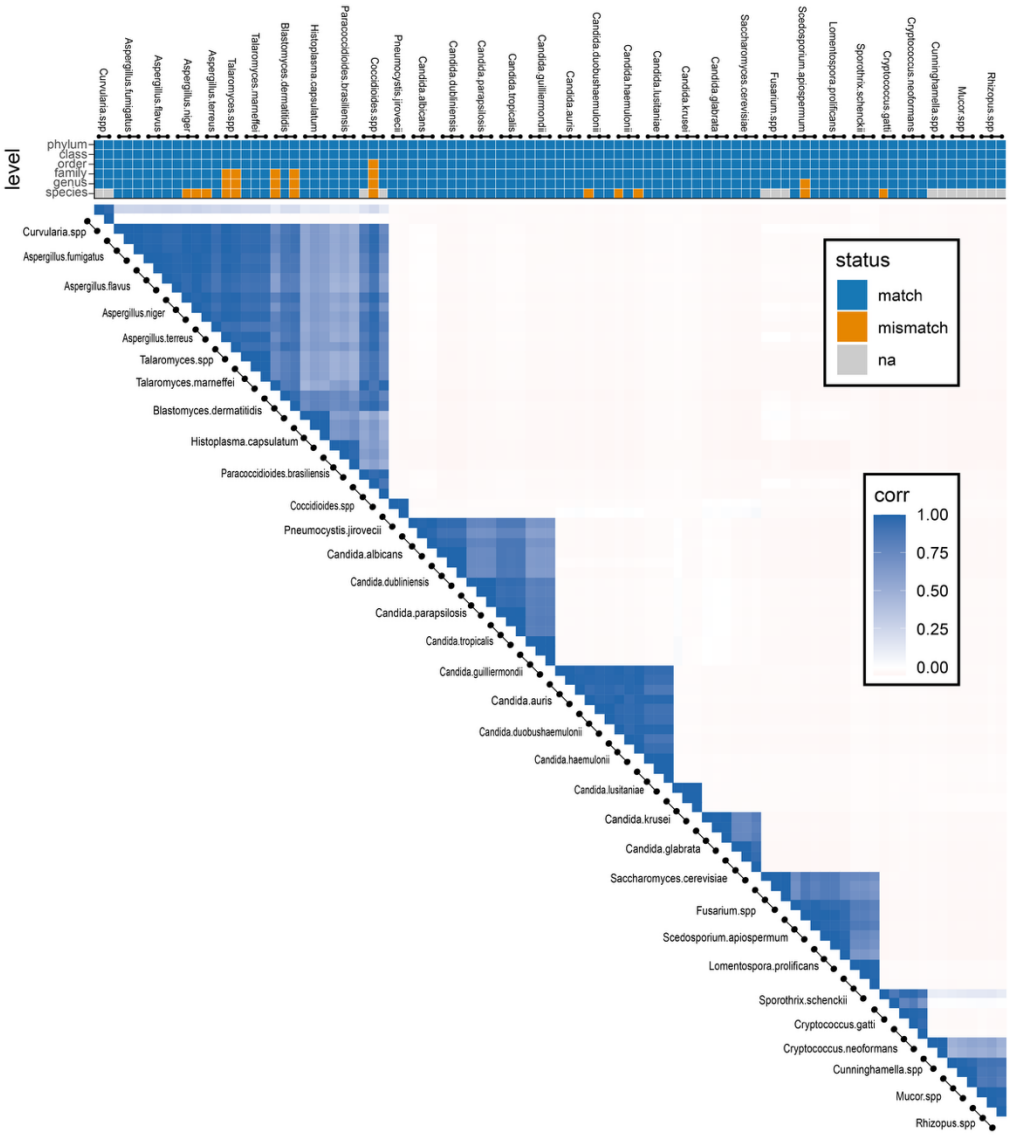

Figure S3. Pearson correlations of Training Set PSRPs are highest between closely related species. Samples with similar taxonomic classification had higher pairwise Pearson correlations than those that were more dissimilar. **(A)** Tile plot indicates prediction accuracy for the single best-matched (highest) non-self-Pearson correlation at each taxonomic level, as in Fig 3a. **(B)** Heatmap of pairwise Pearson correlations, showing that the highest correlations map to members of closely related species. Training Set samples are ordered by taxonomic classification as in Fig 2.

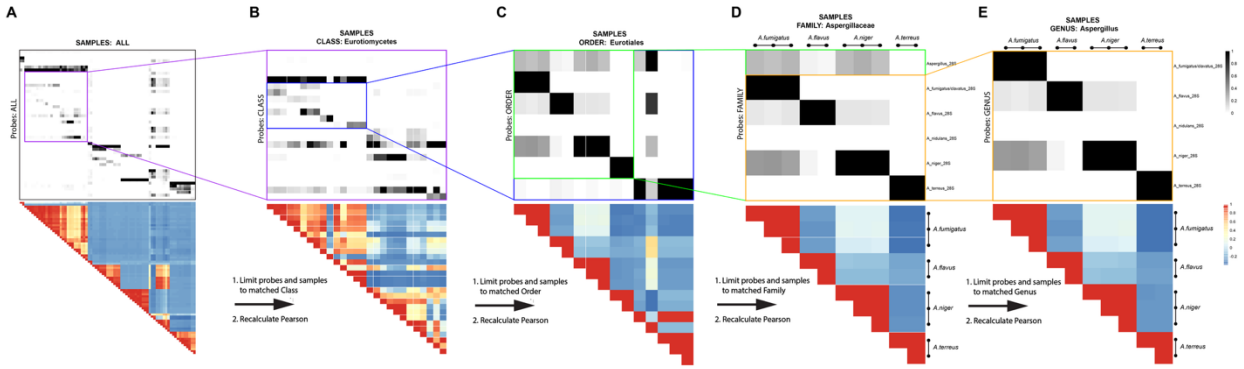

Figure S4. Schematic of our hierarchical Pearson correlation classifier Co-PILOT. Visual representation of how Co-PILOT moves through taxonomic levels, demonstrated on an *Aspergillus fumigatus* sample. Co-PILOT begins by considering all probes and samples **(A)**, and chooses the best-matched class based on the class of the single (non-self) sample with the highest Pearson correlation to the query sample. It then restricts further analysis to only samples from that class, and only probes nested within that class (i.e., those designed to target regions matching an order, family, genus, or species within the selected class), indicated by the box (colored by taxonomic level, as in other figures; here, purple box = class); data from all other samples and probes are removed at this stage **(B)**, including probe(s) matching selected class. In subsequent steps, Co-PILOT selects only the subset of samples & probe(s) containing the best-matched order (B → C, blue box), family (C → D, green box), and genus (D → E, orange box). Top panels = read count heatmaps, rescaled by sample at each step to maximize remaining probe; bottom panels = Pearson correlation heatmaps only using selected data at each step.

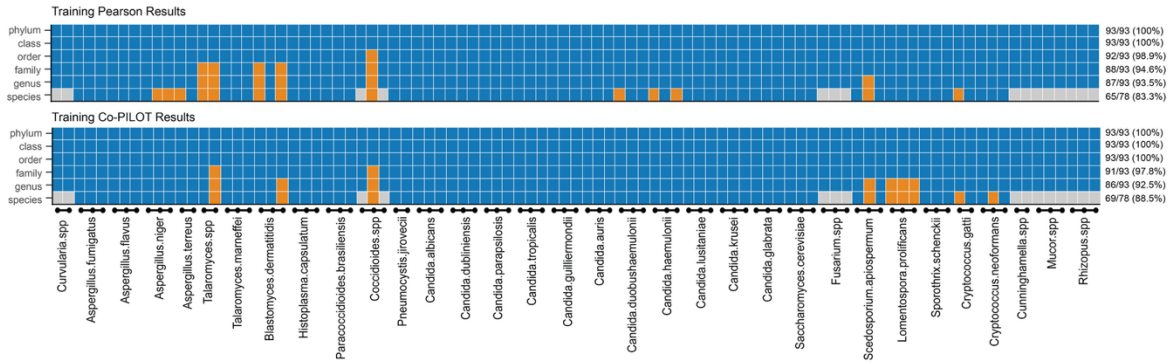

Figure S5. The Co-PILOT classifier improved identification accuracy of the Pan-Fungal Phirst-ID probeset on Training Set. Tile plot indicating prediction accuracy at each taxonomic level, as in Fig 3a. Co-PILOT (bottom panel) improved accuracy relative to simple Pearson correlations (top panel), though it was iteratively designed based on the Training Set, so these results are best viewed as “overtrained” - see main text and Methods for details. By contrast, its performance on the Validation Set (Fig 6) is an independent assessment of Co-PILOT’s accuracy on data it had not seen until its algorithm (Supp Fig S4) was fully designed.

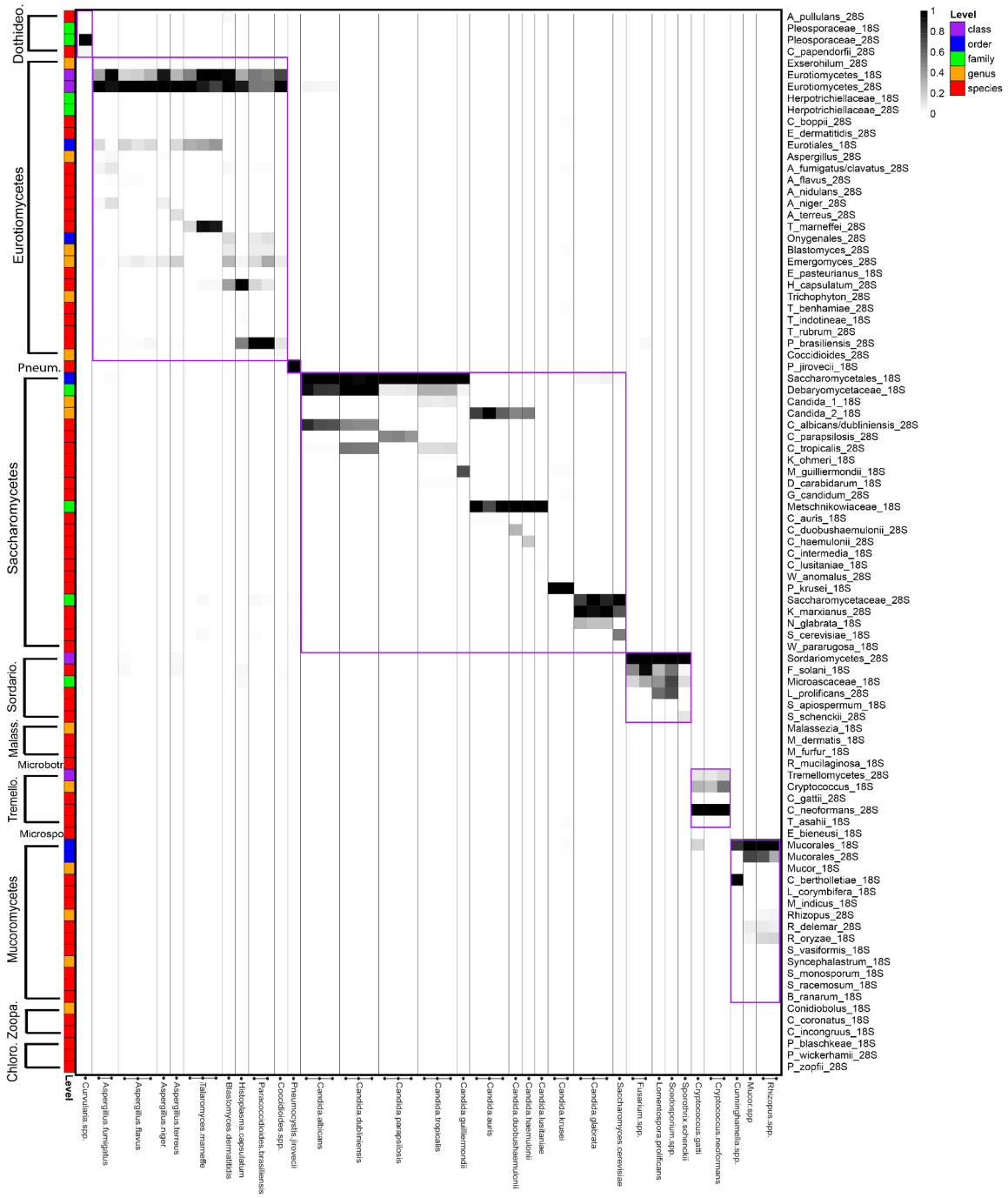

Figure S6. Pan-Fungal Phirst-ID panel generates unique PSRPs for 32 clinically relevant species in our Validation Set. Heatmap of scaled binding intensities of the 54 samples comprising our Validation Set. As in Figure 2, samples and probes are ordered taxonomically, though the cladogram is omitted here. Taxonomic level of each probe is indicated by colored box at left; probe name is listed at right. Purple boxes indicate regions where the class of samples and intended probe targets match.

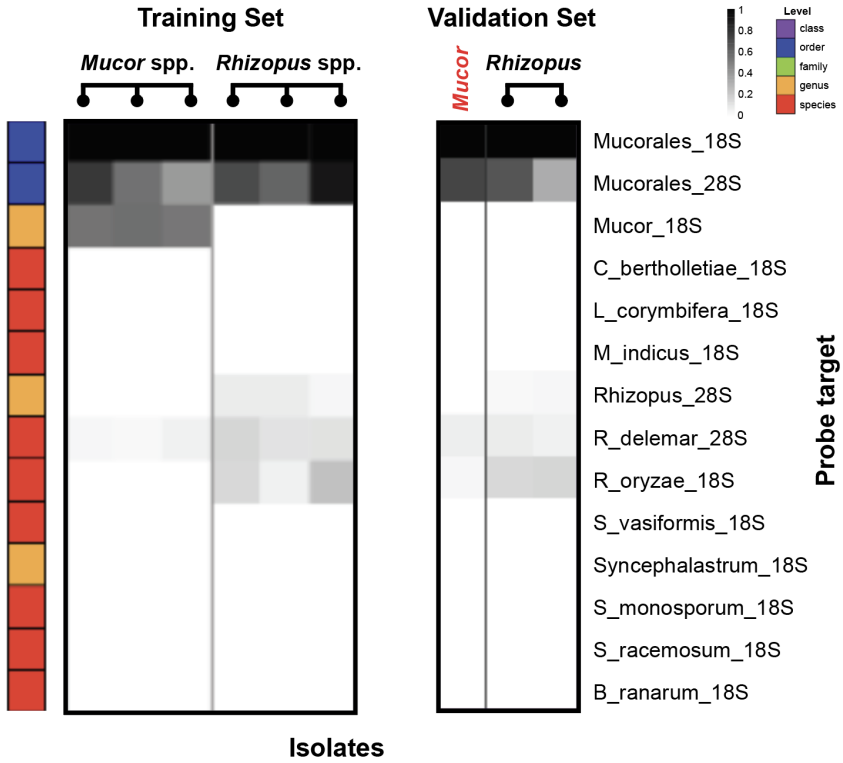

Figure S7 Errant clinical identification of *Mucor* from Validation Set. Pan-Fungal Phirst-ID data from all probes targeting subsets of the *Mucoromycetes* class, shown for all samples from the Training and Validation Sets identified by the clinical microbiology laboratory as either *Mucor* or *Rhizopus*. The red label indicates a Validation sample identified by the clinical laboratory as a *Mucor*, but with a PSRP better resembling a *Rhizopus* (specifically in the lack of Mucor_18S probe reactivity, and perhaps greater R_oryzae_18S probe reactivity). ITS sequencing identified this sample as *Rhizopus microsporus*, more consistent with the Pan-Fungal Phirst-ID prediction than the clinical classification.

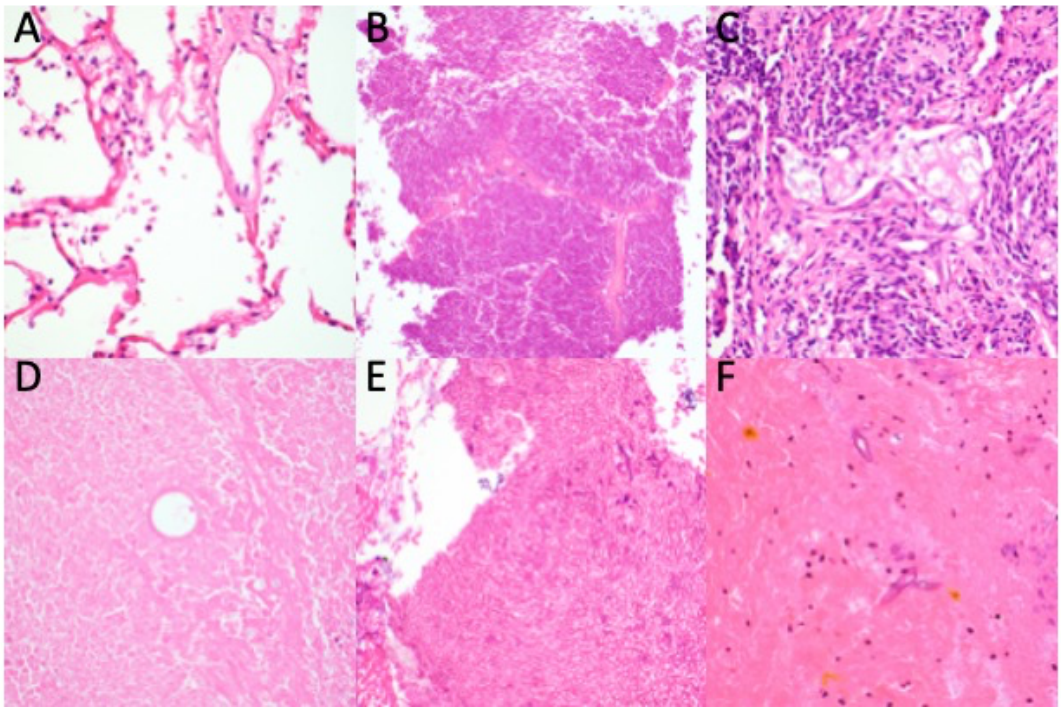

Figure S8. Representative hematoxylin and eosin (H&E)-stained sections from formalin-fixed, paraffin-embedded tissues included in the study (A) Lung tissue, negative control (Fig S9, right panel, column 11; Supp Table S3d, sample FP002). **(B)** Aortic valve tissue with *Candida parapsilosis* (Fig S9, left panel, column 7; Supp Table S3d, sample FP024. **(C)** Lung tissue with *Cryptococcus neoformans* (Fig S9, right panel, column 8; Supp Table S3d, sample FP011). **(D)** Lung tissue with *Coccidioides* sp (Fig S9, right panel, column 4; Supp Table S3d, sample FP019. **(E)** Sinus tissue with *Aspergillus fumigatus* (Fig S9, left panel, column 5; Supp Table S3d, sample FP028). **(F)** Sinus tissue with *Rhizopus* sp (Fig S9, right panel, column 15; Supp Table S3d, sample FP023). All images were acquired using a 40× objective.

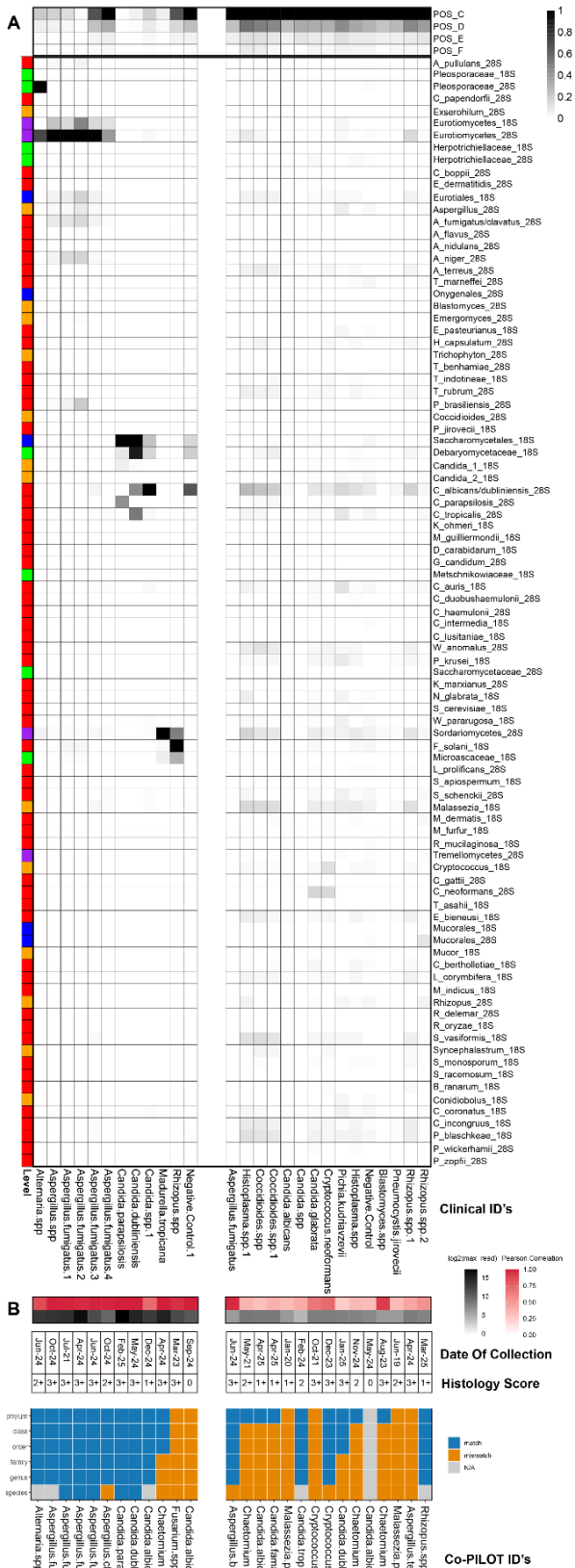
A
POS_C
POS_D
POS_E
POS_F
A_pullulans_28S
Pleosporaceae_18S
Pleosporaceae_28S
C_papendorfii_28S
Exserohilum_28S
Eurotiomycetes_18S
Eurotiomycetes_28S
Herpotrichiellaceae_18S
Herpotrichiellaceae_28S
C_boppii_28S
E_dermatitidis_28S
Eurotiales_18S
Aspergillus_28S
A_fumigatus/clavatus_28S
A_flavus_28S
A_nidulans_28S
A_niger_28S
A_terreus_28S
T_marneffei_28S
Onygenales_28S
Blastomyces_28S
Emergomyces_28S
E_pasteurianus_18S
H_capsulatum_28S
Trichophyton_28S
T_benhamiae_28S
T_indotineae_18S
T_rubrum_28S
P_brasiliensis_28S
Coccidioides_28S
P_jirovecii_18S
Saccharomycetales_18S
Debaryomycetaceae_18S
Candida_1_18S
Candida_2_18S
C_albicans/dubliniensis_28S
C_parapsilosis_28S
C_tropicalis_28S
K_ohmeri_18S
M_guilliermondii_18S
D_carabidarum_18S
G_candidum_28S
Metschnikowiaceae_18S
C_auris_18S
C_duobushaemulonii_28S
C_haemulonii_28S
C_intermedia_18S
C_lusitaniae_18S
W_anomalus_28S
P_krusei_18S
Saccharomycetaceae_28S
K_marxianus_28S
N_glabrata_18S
S_cerevisiae_18S
W_pararugosa_18S
Sordariomycetes_28S
F_solani_18S
Microascaceae_18S
L_prolificans_28S
S_apiospermum_18S
S_schenckii_28S
Malassezia_18S
M_dermatis_18S
M_furfur_18S
R_mucilaginosa_18S
Tremellomycetes_28S
Cryptococcus_18S
C_gattii_28S
C_neoformans_28S
T_asahii_18S
E_bieneusi_18S
Mucorales_18S
Mucorales_28S
Mucor_18S
C_bertholletiae_18S
L_corymbifera_18S
M_indicus_18S
Rhizopus_28S
R_delemar_28S
R_oryzae_18S
S_vasiformis_18S
Syncephalastrum_18S
S_monosporum_18S
S_racemosum_18S
B_ranarum_18S
Conidiobolus_18S
C_coronatus_18S
C_incongruus_18S
P_blaschkeae_18S
P_wickerhamii_28S
P_zopfii_28S
1
0.8
0.6
0.4
0.2
0
Level
class
order
family
genus
species
Level
Alternaria.spp
Aspergillus.spp
Aspergillus.fumigatus.1
Aspergillus.fumigatus.2
Aspergillus.fumigatus.3
Aspergillus.fumigatus.4
Aspergillus.clavatus
Candida.parapsilosis
Candida.dubliniensis
Candida.spp.1
Madurella.tropicana
Rhizopus.spp
Negative.Control.1
Aspergillus.fumigatus
Histoplasma.spp.1
Coccidioides.spp
Coccidioides.spp.1
Candida.albicans
Candida.spp
Candida.glabrata
Cryptococcus.neoformans
Pichia.kudriavzevii
Histoplasma.spp
Negative.Control
Blastomyces.spp
Pneumocystis.jirovecii
Rhizopus.spp.1
Rhizopus.spp.2
Clinical ID's
B
Jun-24 Oct-24 Jul-21 Apr-24 Jun-24 Oct-24 Feb-25 May-24 Dec-24 Apr-24 Mar-23 Sep-24
2+ 3+ 3+ 3+ 3+ 2+ 3+ 3+ 1+ 3+ 3+ 0
Jun-24 May-21 Apr-25 Jan-20 Feb-24 Dec-23 Oct-21 Jan-25 Nov-24 May-24 Aug-23 Jun-19 Apr-24 Mar-25
3+ 2+ 1+ 1+ 2 3+ 3+ 3+ 2 0 3+ 2+ 3+ 1+
log2(max read)
15
10
5
0
Pearson Correlation
1.00
0.75
0.50
0.25
0.00
Date Of Collection
Histology Score
phylum
class
order
family
genus
species
match
mismatch
NA
Alternaria.spp
Aspergillus.fumigatus
Aspergillus.fumigatus
Aspergillus.fumigatus
Aspergillus.fumigatus
Aspergillus.clavatus
Candida.parapsilosis
Candida.dubliniensis
Candida.albicans
Chaetomium
Fusarium.spp
Candida.albicans
Aspergillus.brasiliensis
Chaetomium
Candida.albicans
Candida.famata
Malassezia.pachydermatis
Candida.tropicalis
Cryptococcus.neoformans
Cryptococcus.gattii
Candida.dubliniensis
Chaetomium
Candida.albicans
Chaetomium
Malassezia.pachydermatis
Aspergillus.terreus
Rhizopus.spp
Co-PILOT ID's

Figure S9: Pilot use of Pan-Fungal Phirst ID for FFPE samples (A) Heatmap of scaled probe binding intensities of 27 FFPE samples. For column-scaling to better visually represent total read counts, the four lowest-abundance positive control spike-ins are included for each sample (top 4 rows, above horizontal line). Bottom axis indicates clinical identification provided by the Pathology department (see Supplementary Table S3d). **(B)** Tile plot indicating prediction accuracy of Pan-Fungal Phirst-ID with Co-PILOT at each taxonomic level, as in Fig 3a. Date of sample collected is indicated above and final Co-PILOT identification (best match from Training Set) is listed below the tile plot. 12 samples at left, which exceeded our probe detection threshold, are separated from 17 samples at right, which did not. For visualization purposes, all samples are scaled to the third-most-abundant positive control spike-in (shown above black horizontal line at top). Samples are sorted by taxonomic order of the identification from the clinical microbiology laboratory.

843

844 **Cited Works**

845 1. Almeida, F., Rodrigues, M. L., & Coelho, C. (2019). The Still Underestimated Problem of
846 Fungal Diseases Worldwide. *Frontiers in Microbiology*, *10*.
847 https://doi.org/10.3389/fmicb.2019.00214
848 2. Arvanitis, M., Anagnostou, T., Fuchs, B. B., Caliendo, A. M., & Mylonakis, E. (2014).
849 Molecular and Nonmolecular Diagnostic Methods for Invasive Fungal Infections. *Clinical*
850 *Microbiology Reviews*, *27*(3), 490–526. https://doi.org/10.1128/CMR.00091-13
851 3. Zhang, S. X., Babady, N. E., Hanson, K. E., Harrington, A. T., Larkin, P. M. K., Leal, S.
852 M., Luethy, P. M., Martin, I. W., Pancholi, P., Procop, G. W., Riedel, S., Seyedmousavi, S.,
853 Sullivan, K. V., Walsh, T. J., & Lockhart, S. R. (2021). Recognition of Diagnostic Gaps for
854 Laboratory Diagnosis of Fungal Diseases: Expert Opinion from the Fungal Diagnostics
855 Laboratories Consortium (FDLC). *Journal of Clinical Microbiology*, *59*(7), e01784-20.
856 https://doi.org/10.1128/JCM.01784-20
857 4. Badiee, P., & Hashemizadeh, Z. (2014). Opportunistic invasive fungal infections:
858 Diagnosis & clinical management. *The Indian Journal of Medical Research*, *139*(2), 195–
859 204.
860 5. Kozel, T. R., & Wickes, B. (2014). Fungal diagnostics. *Cold Spring Harbor Perspectives*
861 *in Medicine*, *4*(4), a019299. https://doi.org/10.1101/cshperspect.a019299
862 6. Barnes, R. A. (2008). Early diagnosis of fungal infection in immunocompromised
863 patients. *Journal of Antimicrobial Chemotherapy*, *61*(Supplement 1), i3–i6.
864 https://doi.org/10.1093/jac/dkm424
865 7. Freeman Weiss, Z., Leon, A., & Koo, S. (2021). The Evolving Landscape of Fungal
866 Diagnostics, Current and Emerging Microbiological Approaches. *Journal of Fungi*, *7*(2), 127.
867 https://doi.org/10.3390/jof7020127

868 8. Hage, C. A., Carmona, E. M., Epelbaum, O., Evans, S. E., Gabe, L. M., Haydour, Q.,
869 Knox, K. S., Kolls, J. K., Murad, M. H., Wengenack, N. L., & Limper, A. H. (2019).
870 Microbiological Laboratory Testing in the Diagnosis of Fungal Infections in Pulmonary and
871 Critical Care Practice. An Official American Thoracic Society Clinical Practice Guideline.
872 *American Journal of Respiratory and Critical Care Medicine*, *200*(5), 535–550.
873 https://doi.org/10.1164/rccm.201906-1185ST
874 9. Wickes, B. L., & Wiederhold, N. P. (2018). Molecular diagnostics in medical mycology.
875 *Nature Communications*, *9*(1), 5135. https://doi.org/10.1038/s41467-018-07556-5
876 10. Theel, E. S., & Doern, C. D. (2013). Point-Counterpoint: β- D -Glucan Testing Is
877 Important for Diagnosis of Invasive Fungal Infections. *Journal of Clinical Microbiology*,
878 *51*(11), 3478–3483. https://doi.org/10.1128/JCM.01737-13
879 11. Yaman, G., Akyar, I., & Can, S. (2012). Evaluation of the MALDI TOF-MS method for
880 identification of Candida strains isolated from blood cultures. *Diagnostic Microbiology and*
881 *Infectious Disease*, *73*(1), 65–67. https://doi.org/10.1016/j.diagmicrobio.2012.01.013
882 12. Lau, A. F. (2021). Matrix-Assisted Laser Desorption Ionization Time-of-Flight for Fungal
883 Identification. *Clinics in Laboratory Medicine*, *41*(2), 267–283.
884 https://doi.org/10.1016/j.cll.2021.03.006
885 13. Huang, Y., Zhang, M., Zhu, M., Wang, M., Sun, Y., Gu, H., Cao, J., Li, X., Zhang, S.,
886 Wang, J., & Lu, X. (2017). Comparison of two matrix-assisted laser desorption ionization-
887 time of flight mass spectrometry systems for the identification of clinical filamentous fungi.
888 *World Journal of Microbiology and Biotechnology*, *33*(7), 142.
889 https://doi.org/10.1007/s11274-017-2297-3
890 14. Klugherz, I., Kölli, B., Reinmüller, M., Willinger, B., Leitner, E., Steinmetz, I., & Dichtl, K.
891 (2025). Identification of Filamentous Fungi: An Evaluation of Three MALDI - TOF Mass
892 Spectrometry Systems. *Mycoses*, *68*(6), e70078. https://doi.org/10.1111/myc.70078

15. Kurtzman, C. P., & Robnett, C. J. (1998). Identification and phylogeny of ascomycetous yeasts from analysis of nuclear large subunit (26S) ribosomal DNA partial sequences. *Antonie van Leeuwenhoek*, *73*(4), 331–371. https://doi.org/10.1023/A:1001761008817

16. Cathy A. Petti, MD, Mary E. Brandt, PhD, Deirdre L. Church, MD, PhD, D(ABMM), Stefan Emler, MD, Keith Simmon, MS, PhD, & Adrian M. Zelazny, PhD, D(ABMM). (2018). *Interpretive Criteria for Identification of Bacteria and Fungi by Targeted DNA Sequencing* (2nd ed.). Clinical and Laboratory Standards Institute (CLSI). https://clsi.org/shop/standards/mm18/

17. Alanio, A., & Bretagne, S. (2014). Difficulties with molecular diagnostic tests for mould and yeast infections: Where do we stand? *Clinical Microbiology and Infection*, *20*, 36–41. https://doi.org/10.1111/1469-0691.12617

18. Bhattacharyya, R. P., Walker, M., Boykin, R., Son, S. S., Liu, J., Hachey, A. C., Ma, P., Wu, L., Choi, K., Cummins, K. C., Benson, M., Skerry, J., Ryu, H., Wong, S. Y., Goldberg, M. B., Han, J., Pierce, V. M., Cosimi, L. A., Shoresh, N., … Hung, D. T. (2019). Rapid identification and phylogenetic classification of diverse bacterial pathogens in a multiplexed hybridization assay targeting ribosomal RNA. *Scientific Reports*, *9*(1), 4516. https://doi.org/10.1038/s41598-019-40792-3

19. Geiss, G. K., Bumgarner, R. E., Birditt, B., Dahl, T., Dowidar, N., Dunaway, D. L., Fell, H. P., Ferree, S., George, R. D., Grogan, T., James, J. J., Maysuria, M., Mitton, J. D., Oliveri, P., Osborn, J. L., Peng, T., Ratcliffe, A. L., Webster, P. J., Davidson, E. H., … Dimitrov, K. (2008). Direct multiplexed measurement of gene expression with color-coded probe pairs. *Nature Biotechnology*, *26*(3), 317–325. https://doi.org/10.1038/nbt1385

20. Matzko, M. E., Sephton-Clark, P. C. S., Young, E. L., Jhaveri, T. A., Martinsen, M. A., Mojica, E., Boykin, R., Pierce, V. M., Cuomo, C. A., & Bhattacharyya, R. P. (2022). A novel rRNA hybridization-based approach to rapid, accurate *Candida* identification directly from blood culture. *Medical Mycology*, *60*(9), myac065. https://doi.org/10.1093/mmy/myac065

21. Voorhies, M., Cohen, S., Shea, T. P., Petrus, S., Muñoz, J. F., Poplawski, S., Goldman, W. E., Michael, T. P., Cuomo, C. A., Sil, A., & Beyhan, S. (2022). Chromosome-Level Genome Assembly of a Human Fungal Pathogen Reveals Synteny among Geographically Distinct Species. *mBio*, *13*(1), e02574-21. https://doi.org/10.1128/mbio.02574-21

22. Cuomo, C. A., Rodriguez-Del Valle, N., Perez-Sanchez, L., Abouelleil, A., Goldberg, J., Young, S., Zeng, Q., & Birren, B. W. (2014). Genome Sequence of the Pathogenic Fungus Sporothrix schenckii (ATCC 58251). *Genome Announcements*, *2*(3), e00446-14. https://doi.org/10.1128/genomeA.00446-14

23. Sephton-Clark, P., Nguyen, T., Hoa, N. T., Ashton, P., van Doorn, H. R., Ly, V. T., Le, T., & Cuomo, C. A. (2023). Impact of pathogen genetics on clinical phenotypes in a population of Talaromyces marneffei from Vietnam. *Genetics*, *224*(4), iyad100. https://doi.org/10.1093/genetics/iyad100

24. Muñoz, J. F., Gauthier, G. M., Desjardins, C. A., Gallo, J. E., Holder, J., Sullivan, T. D., Marty, A. J., Carmen, J. C., Chen, Z., Ding, L., Gujja, S., Magrini, V., Misas, E., Mitreva, M., Priest, M., Saif, S., Whiston, E. A., Young, S., Zeng, Q., … Cuomo, C. A. (2015). The Dynamic Genome and Transcriptome of the Human Fungal Pathogen Blastomyces and Close Relative Emmonsia. *PLoS Genetics*, *11*(10), e1005493. https://doi.org/10.1371/journal.pgen.1005493

25. Muñoz, J. F., Gallo, J. E., Misas, E., Priest, M., Imamovic, A., Young, S., Zeng, Q., Clay, O. K., McEwen, J. G., & Cuomo, C. A. (2014). Genome update of the dimorphic human pathogenic fungi causing paracoccidioidomycosis. *PLoS Neglected Tropical Diseases*, *8*(12), e3348. https://doi.org/10.1371/journal.pntd.0003348

26. Hudson, J., Budvytiene, I., & Banaei, N. (2025). Diagnostic stewardship applied to targeted fungal sequencing. *Journal of Clinical Microbiology*, *63*(10), e00896-25. https://doi.org/10.1128/jcm.00896-25

27. Leaw, S. N., Chang, H. C., Sun, H. F., Barton, R., Bouchara, J.-P., & Chang, T. C. (2006). Identification of Medically Important Yeast Species by Sequence Analysis of the Internal Transcribed Spacer Regions. *Journal of Clinical Microbiology*, *44*(3), 693–699. https://doi.org/10.1128/JCM.44.3.693-699.2006

28. Abarenkov, K., Nilsson, R. H., Larsson, K.-H., Taylor, A. F. S., May, T. W., Frøslev, T. G., Pawlowska, J., Lindahl, B., Põldmaa, K., Truong, C., Vu, D., Hosoya, T., Niskanen, T., Piirmann, T., Ivanov, F., Zirk, A., Peterson, M., Cheeke, T. E., Ishigami, Y., … Kõljalg, U. (2024). The UNITE database for molecular identification and taxonomic communication of fungi and other eukaryotes: Sequences, taxa and classifications reconsidered. *Nucleic Acids Research*, *52*(D1), D791–D797. https://doi.org/10.1093/nar/gkad1039

29. Poplin, V., Smith, C., Caceres, D. H., Herkert, P. F., Jegede, O., Thompson, G. R., Baddley, J. W., Schwartz, I. S., Kubat, R., Deka, M. A., Toda, M., Lockhart, S. R., Chiller, T., Hagen, F., & Bahr, N. C. (2024). Geographical distribution of the Cryptococcus gattii species complex: A systematic review. *The Lancet. Microbe*, *5*(12), 100921. https://doi.org/10.1016/S2666-5247(24)00161-7

30. Kwon-Chung, K. J., Bennett, J. E., Wickes, B. L., Meyer, W., Cuomo, C. A., Wollenburg, K. R., Bicanic, T. A., Castañeda, E., Chang, Y. C., Chen, J., Cogliati, M., Dromer, F., Ellis, D., Filler, S. G., Fisher, M. C., Harrison, T. S., Holland, S. M., Kohno, S., Kronstad, J. W., … Casadevall, A. (2017). The Case for Adopting the “Species Complex” Nomenclature for the Etiologic Agents of Cryptococcosis. *mSphere*, *2*(1), e00357-16. https://doi.org/10.1128/mSphere.00357-16

31. Lackner, M., De Hoog, G. S., Yang, L., Ferreira Moreno, L., Ahmed, S. A., Andreas, F., Kaltseis, J., Nagl, M., Lass-Flörl, C., Risslegger, B., Rambach, G., Speth, C., Robert, V., Buzina, W., Chen, S., Bouchara, J.-P., Cano-Lira, J. F., Guarro, J., Gené, J., … Liporagi Lopes, L. C. (2022). Proposed nomenclature for Pseudallescheria, Scedosporium and

969 related genera. *Fungal Diversity*, *113*(1), 193–194. https://doi.org/10.1007/s13225-022-
970 00505-0
971 32. Sangoi, A. R., Rogers, W. M., Longacre, T. A., Montoya, J. G., Baron, E. J., & Banaei, N.
972 (2009). Challenges and Pitfalls of Morphologic Identification of Fungal Infections in
973 Histologic and Cytologic Specimens. *American Journal of Clinical Pathology*, *131*(3), 364–
974 375. https://doi.org/10.1309/AJCP99OOOZSNISCZ
975 33. Safiia, J., Díaz, M. A., Alshaker, H., Atallah, C. J., Sakr, P., Moshovitis, D. G., Nawlo, A.,
976 Franceschi, A. E., Liakos, A., & Koo, S. (2024). Recent Advances in Diagnostic Approaches
977 for Mucormycosis. *Journal of Fungi*, *10*(10), 727. https://doi.org/10.3390/jof10100727
978 34. Mathieson, W., & Thomas, G. A. (2020). Why Formalin-fixed, Paraffin-embedded
979 Biospecimens Must Be Used in Genomic Medicine: An Evidence-based Review and
980 Conclusion. *The Journal of Histochemistry and Cytochemistry: Official Journal of the*
981 *Histochemistry Society*, *68*(8), 543–552. https://doi.org/10.1369/0022155420945050
982 35. Fox, C. H., Johnson, F. B., Whiting, J., & Roller, P. P. (1985). Formaldehyde fixation.
983 *The Journal of Histochemistry and Cytochemistry: Official Journal of the Histochemistry*
984 *Society*, *33*(8), 845–853. https://doi.org/10.1177/33.8.3894502
985 36. Guarner, J., & Brandt, M. E. (2011). Histopathologic Diagnosis of Fungal Infections in
986 the 21st Century. *Clinical Microbiology Reviews*, *24*(2), 247–280.
987 https://doi.org/10.1128/CMR.00053-10
988 37. Cabaret, O., Toussain, G., Abermil, N., Alsamad, I. A., Botterel, F., Costa, J.-M., Papon,
989 J.-F., & Bretagne, S. (2011). Degradation of fungal DNA in formalin-fixed paraffin-embedded
990 sinus fungal balls hampers reliable sequence-based identification of fungi. *Medical*
991 *Mycology*, *49*(3), 329–332. https://doi.org/10.3109/13693786.2010.525537
992 38. Gomez, C. A., Budvytiene, I., Zemek, A. J., & Banaei, N. (2017). Performance of
993 Targeted Fungal Sequencing for Culture-Independent Diagnosis of Invasive Fungal
994 Disease. *Clinical Infectious Diseases*, *65*(12), 2035–2041. https://doi.org/10.1093/cid/cix728

39. Lænkholm, A.-V., Jensen, M.-B., Eriksen, J. O., Rasmussen, B. B., Knoop, A. S., Buckingham, W., Ferree, S., Schaper, C., Nielsen, T. O., Haffner, T., Kibøl, T., Møller Talman, M.-L., Bak Jylling, A. M., Tabor, T. P., & Ejlertsen, B. (2018). PAM50 Risk of Recurrence Score Predicts 10-Year Distant Recurrence in a Comprehensive Danish Cohort of Postmenopausal Women Allocated to 5 Years of Endocrine Therapy for Hormone Receptor–Positive Early Breast Cancer. *Journal of Clinical Oncology*, *36*(8), 735–740. https://doi.org/10.1200/JCO.2017.74.6586

40. Costa, R. L. B., & Gradishar, W. J. (2018). Do Genomic Assays Provide the Necessary Confidence to De-escalate Adjuvant Therapy? *Journal of Clinical Oncology*, *36*(8), 725–727. https://doi.org/10.1200/JCO.2017.76.9802

41. Gnant, M., Sestak, I., Filipits, M., Dowsett, M., Balic, M., Lopez-Knowles, E., Greil, R., Dubsky, P., Stoeger, H., Rudas, M., Jakesz, R., Ferree, S., Cowens, J. W., Nielsen, T., Schaper, C., Fesl, C., & Cuzick, J. (2015). Identifying clinically relevant prognostic subgroups of postmenopausal women with node-positive hormone receptor-positive early-stage breast cancer treated with endocrine therapy: A combined analysis of ABCSG-8 and ATAC using the PAM50 risk of recurrence score and intrinsic subtype. *Annals of Oncology*, *26*(8), 1685–1691. https://doi.org/10.1093/annonc/mdv215

42. Khot, P. D., Ko, D. L., & Fredricks, D. N. (2009). Sequencing and analysis of fungal rRNA operons for development of broad-range fungal PCR assays. *Applied and Environmental Microbiology*, *75*(6), 1559–1565. https://doi.org/10.1128/AEM.02383-08

43. Kwon-Chung, K. J., Fraser, J. A., Doering, T. L., Wang, Z., Janbon, G., Idnurm, A., & Bahn, Y.-S. (2014). Cryptococcus neoformans and Cryptococcus gattii, the etiologic agents of cryptococcosis. *Cold Spring Harbor Perspectives in Medicine*, *4*(7), a019760. https://doi.org/10.1101/cshperspect.a019760

44. Wu, Y., Grossman, N., Totten, M., Memon, W., Fitzgerald, A., Ying, C., & Zhang, S. X. (2020). Antifungal Susceptibility Profiles and Drug Resistance Mechanisms of Clinical

1021 Lomentospora prolificans Isolates. *Antimicrobial Agents and Chemotherapy*, *64*(11),
1022 e00318-20. https://doi.org/10.1128/AAC.00318-20
1023 45. Chen, S. C.-A., Halliday, C. L., Hoenigl, M., Cornely, O. A., & Meyer, W. (2021).
1024 Scedosporium and Lomentospora Infections: Contemporary Microbiological Tools for the
1025 Diagnosis of Invasive Disease. *Journal of Fungi*, *7*(1), 23.
1026 https://doi.org/10.3390/jof7010023
1027 46. Aggarwal, D., Kanitkar, T., Narouz, M., Azadian, B. S., Moore, L. S. P., & Mughal, N.
1028 (2020). Clinical utility and cost-effectiveness of bacterial 16S rRNA and targeted PCR based
1029 diagnostic testing in a UK microbiology laboratory network. *Scientific Reports*, *10*(1), 7965.
1030 https://doi.org/10.1038/s41598-020-64739-1
1031 47. Kubiak, J., Morgan, A., Kirmaier, A., Arnaout, R., & Riedel, S. (2023). Universal PCR for
1032 bacteria, mycobacteria, and fungi: A 10-year retrospective review of clinical indications and
1033 patient outcomes. *Journal of Clinical Microbiology*, *61*(12), e00952-23.
1034 https://doi.org/10.1128/jcm.00952-23
1035 48. Kerkhoff, A. D., Rutishauser, R. L., Miller, S., & Babik, J. M. (2020). Clinical Utility of
1036 Universal Broad-Range Polymerase Chain Reaction Amplicon Sequencing for Pathogen
1037 Identification: A Retrospective Cohort Study. *Clinical Infectious Diseases*, *71*(6), 1554–1557.
1038 https://doi.org/10.1093/cid/ciz1245
1039 49. Naureckas Li, C., & Nakamura, M. M. (2022). Utility of Broad-Range PCR Sequencing
1040 for Infectious Diseases Clinical Decision Making: A Pediatric Center Experience. *Journal of*
1041 *Clinical Microbiology*, *60*(5), e02437-21. https://doi.org/10.1128/jcm.02437-21
1042 50. Weinert-Stein, K., Cater, M., Cherian, S. S., Azem, R., Khazan, A. E., Desai, A. P.,
1043 Tripp, L., Lim, P. P., Stempak, L. M., & Hojat, L. S. (2024). Clinical Utility of Broad-Range
1044 PCR Testing and Impact on Outcomes in Adults with Suspected Infection. *Antibiotics*,
1045 *13*(12), 1166. https://doi.org/10.3390/antibiotics13121166
1046